Transient climate response to Arctic sea-ice loss with two ice-constraining methods

Amélie Simon, Guillaume Gastineau, Claude Frankignoul, Clément Rousset, Francis Codron

Transient climate response to Arctic sea-ice loss with two ice-constraining methods

Amélie Simon*, Guillaume Gastineau, Claude Frankignoul,

Clément Rousset and Francis Codron

Sorbonne Université/IRD/MNHN/CNRS, LOCEAN, Paris, France

September 22, 2020

Submitted to Journal of Climate

*Corresponding author address: Dr Amélie Simon, Sorbonne Université/IRD /MNHN/CNRS, LOCEAN/IPSL, 4 place Jussieu, 75005 Paris, France.

E-mail: amelie.simon@locean-ipsl.upmc.fr

Abstract

The impact of Arctic sea-ice loss on the ocean and atmosphere is investigated focusing on a gradual reduction of Arctic sea-ice by 20% on annual mean, occurring within 30 years, starting from present-day conditions. Two ice-constraining methods are explored to melt Arctic sea-ice in a coupled climate model, while keeping present-day conditions for external forcing. The first method uses a reduction of sea-ice albedo, which modifies the incoming surface shortwave radiation. The second method uses a reduction of thermal conductivity, which changes the heat conduction flux inside ice. The reduction of the thermal conductivity inhibits winter oceanic cooling and sea-ice basal growth, thereby reduces seasonality of sea-ice thickness. For similar Arctic sea-ice area loss, decreasing the albedo induces larger Arctic warming than reducing the conductivity, especially in spring. Both ice-constraining methods produce similar climate impacts, but with smaller anomalies when reducing the conductivity. In the Arctic, the sea-ice loss leads to an increase of the North Atlantic water inflow in the Barents Sea and Eastern Arctic, while the salinity decreases and the gyre intensifies in the Beaufort Sea. In the North Atlantic, the subtropical gyre shifts southward and the Atlantic meridional overturning circulation weakens. A dipole of sea-level pressure anomalies sets up in the cold season over Northern Siberia and the North Atlantic, which resembles the negative phase of the North Atlantic Oscillation. In the tropics, the Atlantic Intertropical Convergence Zone shifts southward as the South Atlantic Ocean warms up, Walker circulation reorganizes and the Southeastern Pacific Ocean cools down.

1. Introduction

The Arctic is a region of pronounced climate change. Since the mid 20th century, the Arctic has warmed more than twice as fast as the rest of the planet (e.g., Bluenden and Arndt, 2012), a phenomenon referred to as Arctic Amplification. The Intergovernmental Panel on Climate Change (IPCC) Special Report on the Ocean and Cryosphere in a Changing Climate (Pörtner et al., 2019) concluded that over the 1979-2018 period the Arctic sea-ice extent has shrunk in all months of the year with a maximum decrease in September, with a reduction of about 13 % per decade. Also, the Arctic sea-ice has thinned and the area of multi-year ice has declined by about 90 %. These trends are expected to increase in the future. The multi-model mean of the representative concentration pathway (RCP) 8.5 scenario projected a summer ice-free Arctic in the coupled model intercomparison project version 5 (CMIP5; Stocker et al., 2013) by 2060 and in the version 6 (CMIP6; SIMIP community, 2020) by 2050.

The influence of Arctic sea-ice decline on global climate remains under debate (Cohen et al., 2014), in particular its influence on mid-latitudes (Overland et al., 2013). Observational studies have linked Arctic sea-ice loss in late autumn to a negative North Atlantic Oscillation in winter (NAO; King et al., 2016; Garcia-Serrano et al., 2015; Simon et al., 2020), but there is still discussion on the robustness and pathway of this sea-ice influence. As the observational records are short, climate models have been extensively used. Among atmospheric general circulation model (AGCM) studies, there is no consensus on the atmospheric response to sea-ice loss. Some studies (Singayayer et al., 2006; Strey et al., 2010) found no NAO-like pattern as a response to Arctic sea-ice loss, while others found a positive NAO response in winter (Screen et al., 2014) or both autumn and winter (Cassano et al., 2014). Besides, others studies show a negative NAO response to Arctic sea-ice decline, but with different seasonality: larger in early spring (Seierstad et al., 2009; Sun et al. 2015), in winter (Magnusdottir et al., 2004; Peings and Magnusdottir, 2014) or only in February (Deser et al., 2010b). Among atmosphere-ocean general circulation model (AOGCM) studies, there is a broader consensus on a negative NAO-like response in winter (Deser et al., 2015; Blackport and Kushner, 2016; Blackport and Kushner, 2017; McCusker et al., 2017; Oudar et al., 2017; Smith et

al., 2017; Suo et al., 2017; Screen et al., 2018). In the ocean, observational and modelling studies found a strengthened North Atlantic inflow and weaker stratification in the Barents Sea and the Eastern Arctic, a phenomenon called “Atlantification”, reinforcing the sea-ice loss (Årthun et al., 2012; Polyakov et al., 2017; Barton et al., 2018). However, it is still unclear how and at which rate the Arctic ocean salinity, temperature and stratification will be modified (Wassmann et al., 2015; Lind et al., 2018). In AOGCMs, the Arctic sea-ice decline also weakens the Atlantic Meridional Overturning Circulation (AMOC; Oudar et al., 2017; Sévellec et al., 2017; Suo et al., 2017; Sun et al., 2018; Wang et al., 2018; Liu et al., 2019) because of freshwater release and modified surface heat fluxes in the Arctic-North Atlantic region. However, the relative importance of each process remains unclear.

The impacts of Arctic sea-ice loss are not confined to the North Atlantic in coupled models where ocean-atmosphere coupled feedbacks are accounted for. Deser et al. (2015) showed that the impact of Arctic sea-ice loss then becomes global. However, the large-scale response is not unanimous. Most previous studies (Deser et al., 2010b; Deser et al., 2015; Blackport and Kushner, 2016; Sévellec et al., 2017; Oudar et al., 2017; Suo et al., 2017; Monerie et al., 2019; Screen et al., 2018, Sun et al., 2018, Liu and Fedorov, 2019; England et al., 2020; Sun et al., 2020) found a tropical warming with the largest warming in the Central Pacific, similar to the greenhouse gas-driven warming. This warming called "mini-global warming" in Deser et al. (2015), is associated with an intensified Aleutian Low in winter. However, the fast transient response to sea-ice loss was found to be less robust when the ocean circulation is not fully adjusted, typically after one to five decades following a sea-ice perturbation. Blackport and Screen, 2019 found no change in the Aleutian Low with 5-years-long simulations. In Wang et al. (2018), the Equatorial Pacific and the Southern Ocean are hardly modified in the first decades of their AOGCM simulation or when using a slab-ocean instead of a full ocean model. Cvijanovic et al. (2017) rather found a cooling of the Southeastern Pacific, with their climate model simulations based on both slab-ocean and full-ocean configurations. Blackport and Kushner (2016), as well as Liu and Fedorov (2019), also found different oceanic and atmospheric responses in the early (first decades) and late period (after one

century) of their simulations, while Sun et al. (2018) found generally similar responses. The reason for the discrepancy in the transient Pacific response is still under debate.

Some of these studies used a relatively large sea-ice perturbation yielding an ice-free Arctic during two to four months (Deser et al., 2015; Blackport et al., 2017; Oudar et al., 2017; Suo et al. 2017; Sun et al., 2020). However, there is also a need to estimate the impact of smaller Arctic sea-ice loss, for which the Arctic Ocean in September is not ice-free in September, as in (Blackport et al., 2016; Blackport et al., 2017; Cvijanovic et al., 2017; Blackport and Screen, 2019). As the climate of the next decades is an important threshold for a wide range of climate impacts (Masson-Delmotte et al., 2018), we investigate next a moderate Arctic sea-ice loss, corresponding to a loss of 20% on annual mean and 50% reduction in September. As we will detail later, this corresponds to a reduction expected to occur in approximately 2040.

Another open question concerns abrupt versus gradual sea-ice reduction. One can argue that the transient climate response to an abrupt Arctic sea-ice retreat occurring within a few years would change if the climate system had more time to adjust. As in Sun et al. (2018), we will impose a gradual sea-ice loss, comparable to that found in scenario simulations.

Many different methods have been used to constrain sea-ice in AOGCMs: nudging (McCusker et al. 2017; Smith et al., 2017; Suo et al., 2017), flux adjustment (Oudar et al. 2017; Monerie et al., 2019), ghost forcing/ice-nudging (Deser et al., 2015; Deser et al., 2016; Tomas et al., 2016; Sun et al., 2020), sea-ice/snow albedos or emissivity modifications (Deser et al., 2015; Blackport et al., 2016; Blackport et al., 2017; Sévellec et al., 2017; Blackport and Screen, 2019; Liu and Fedorov, 2019), Arctic Ocean albedo modification (Cvijanovic et al., 2015) or changing sea-ice physics parameters with large uncertainties (Cvijanovic et al., 2017). However, sea-ice and snow thermal conductivity is also a key parameter for melting and growth, and we evaluate next the ability of thermal conductivity modification to constrain sea-ice. Also, the sensitivity of the climate response to the methodology remains poorly evaluated, as most previous studies use a single model and only

use one method. Recently Sun et al. (2020) compared the albedo method with ice-flux nudging and found an identical equilibrium global climate response. Blackport and Screen (2019) impose two different albedos parameters (albedo of cold deep snow on top of sea-ice or albedo of snow-free ice) which leads to different seasonal cycles of Arctic sea-ice extent. We will similarly investigate two different methods but focusing on the fast climate response. We show that both methods induce qualitatively similar local and remote transient climate responses, but with different magnitude of Arctic warming. The remote responses to sea-ice reduction simulate in both cases a relative cooling of the Southeastern Pacific Ocean.

In section 2, the methodology and experimental protocol are detailed. Two ice-constraining methods are presented, and their similarities and differences are discussed. The Arctic and North Atlantic responses to the Arctic sea-ice retreat are discussed in section 3, while section 4 focuses on global changes. Conclusion and discussion follow in section 5.

2. Methodology

2.1. Model description

We perform simulations with the coupled atmosphere-ocean general circulation model IPSL-CM5A2 (called here CM5A2; Sepulchre et al., 2019), a modified version of IPSL-CM5A-LR (called here CM5A; Dufresne et al., 2013) which was used for CMIP5. CM5A2 uses the same resolution and physical package as CM5A, but it includes an optimized hybrid parallelization to obtain better computing performances, and a modified tuning to reduce the cold bias of CM5A in global surface air temperature.

The atmospheric component is the LMDZ5A model (Hourdin et al., 2012), with a resolution of ~3.7° in longitude and ~1.9° in latitude and 39 vertical levels up to 4 Pa. The land surface module is ORCHIDEE (Krinner et al., 2005). The ocean and sea-ice are simulated by the NEMOv3.6 model (Nucleus for European Modelling of the Ocean; Madec et. al, 2008), using the ORCA2 grid with 182x149 cells, corresponding to a nominal resolution of 2°, and 31 levels. The ocean biochemistry

is modelled by PISCES (Aumont and Bopp, 2006). Sea-ice dynamics and thermodynamics are represented by the LIM2 model (Fichefet and Maqueda, 1997; Fichefet and Maqueda, 1999), a single ice-category model with three layers (one for snow and two for sea-ice) for heat storage and vertical heat conduction.

As shown in Sepulchre et al. (2019), CM5A2 is realistic in many aspects but, as in many low-resolution coupled models, the Gulf Stream and the North Atlantic current are too zonal, generating a cold bias in the North Atlantic sea-surface temperature (SST) of about -2°C and up to -5°C. The AMOC is underestimated with a mean value of 12 ± 1.1 Sv (from 30°S to 60° N) in pre-industrial conditions, compared to observational estimates around 19 Sv (Cunningham et al., 2007). This weak AMOC has been linked to a lack of convection in the Labrador Sea, which is covered by sea-ice in winter. The main deep-water formation sites are instead located in the Greenland Sea and south of Iceland.

The rainfall in CM5A2 is largely similar to CM5A (Sepulchre et al. 2019). In both versions, there is an overestimation of rainfall in the Southern Tropics, leading to the “double ITCZ” (Intertropical Convergence Zone), and an underestimation in the mid-latitudes (20°N-40°N).

In the version CM5A, September (minimum) and March (maximum) Arctic sea-ice area and thickness are overestimated, albeit this remains within the range of CMIP5 models (Maslowski et al., 2012; Stroeve et al., 2012; Kirchmeier et al., 2017)**.** In the updated version CM5A2, sea-ice extent has been improved in the North Atlantic sector. During the 1979-2005 period of a historical run, the September mean Arctic sea-ice extent is about 5.8 10^6 km2 (Fig. 1) and the annual thickness is 2.5 m (not shown). The sea-ice extent is calculated as the total area of all grid cells with at least 15% sea-ice concentration. This compares well with the respective observed value for the same period: 5.5 10^6 km2 (Fig. 1; Cavalieri et al., 1996) and about 2 m (Schweiger et al., 2011).

2.2 Experimental protocol

For reference, we first run a control ensemble of 10 members with CM5A2 for 30 years, called CTRL. The greenhouse gases, aerosols, ozone and land-use are kept constant at the level of the year

2000. Ten initial atmospheric conditions are chosen randomly from a stabilized present-day control run starting from a 500-yr spin-up simulation in pre-industrial conditions. Oceanic initial conditions are identical and correspond to year 90 of this control run. In a 2500-years pre-industrial control of the CM5A model, the indices of Pacific Decadal Oscillation (PDO), Atlantic Multidecadal Oscillation (AMO) and AMOC have autocorrelation with e-folding time smaller than 10-yr (Fig. S1). Therefore, we speculate that oceanic initial conditions would not affect the 10-30 year response investigated here. Hereafter, we discard the first 10 years unless stated otherwise.

Figure 1 displays the observed sea-ice extent calculated from the monthly sea-ice concentration (SIC) based on passive microwave measurements with a 25-km resolution from January 1979 to February 2017 from *National Snow & Ice Data Center* (NSIDC; Cavalieri et al., 1996). The missing values of December 1987 and January 1988 are set to November 1987. It shows that over the last 40 years, the September sea-ice extent has reduced by about 50%. The CTRL simulation and the existing historical experiments both show similar mean September sea-ice extent, with values corresponding to that occurring in the 1980-2005 period. As no scenario runs were available with the CM5A2 version, we use the ones done with CM5A for CMIP5. To meet a 50 % September reduction, we use as a target the sea-ice extent simulated in the ensemble mean of the four CM5A RCP8.5 members averaged over the period 2035-2055, called TARGET. As CM5A shows a large cold bias in the Arctic, the sea-ice target is only slightly larger to the reduction occurred in the last 40 years.

Two reduced Arctic sea-ice ensembles are then constructed by modifying Arctic sea-ice properties, while the Southern Hemisphere sea-ice remains unconstrained. To induce sea-ice melt while ensuring energy and water conservation, we either modify the sea-ice and snow above the sea-ice (the continental snow properties are unconstrained) albedos or their thermal conductivity. Reducing the ice and snow albedos increases sea-ice melt in spring and summer, while reducing the thermal conductivity mainly reduces the sea-ice growth in winter. Indeed, when thermal conductivity is reduced, the sea-ice and snow more effectively insulate the ocean from the atmosphere, so the ocean

(which is at the freezing point) loses less heat in winter and sea-ice basal growth reduces.

To determine the sea-ice and snow albedos needed to reproduce the targeted Arctic sea-ice loss without changing the external forcing, we first use linear regressions, as described in Deser et al. (2015). Starting from the same initial conditions than the CTRL, we run eight 30-year simulations with sea-ice and snow albedo reductions ranging from 0% to 70%. After excluding the first 10 years, linear regressions between August-September-October (ASO) Arctic sea-ice area (SIA) and albedo reduction (blue dots in Fig. 2) provide a rough first estimate of the albedo reduction needed to reproduce the ASO Arctic SIA value of TARGET (~3.5 10^6 km^2; Fig. 2 top-left). We then repeat simulations with albedos closer to this initial estimate. To reduce the uncertainty associated with internal climate variability, we use 5-member ensembles (green squares in Fig. 2), then 10-member ensembles (yellow stars in Fig. 2) with albedo values close to the first estimated value. A reduction of -22.6% for the albedo of Arctic sea-ice and snow best reproduces the targeted SIA. The same process is followed for the reduced thermal conductivity (Fig. 2, top-right), and a reduction of 33% is then needed from the thermal conductivity of Arctic sea-ice and snow.

In the following, we will therefore focus on two experiments based on the previous results. The first ensemble is identical to CTRL except for the Arctic sea-ice and snow albedos reduced by 22.6% and is called ALB. The second one is identical to CTRL, but with Arctic sea-ice and snow thermal conductivity reduced by 33% is called THCD. Both ensembles consist of 10 members of 30-yr. The first 10-yr is discarded. In the following, the impact of the Arctic sea-ice reduction is assessed by comparing the ensemble-means between ALB (or THCD) and CTRL. Statistical significance is estimated using Student *t*-tests for the difference of means, assuming all members are independent.

Lastly, we note that the sensitivity of winter January-February-March (JFM) SIA to albedo and thermal conductivity is different (Fig. 2, bottom). As the albedo modification is acting mostly in summer, a larger albedo reduction of about -45% is needed to reproduce the winter sea-ice area. Interestingly, a reduction of thermal conductivity of about -30% is needed to simulate the JFM sea-ice area, a value similar to that found when using ASO as a target (-33%), suggesting that the seasonal cycle of sea-ice loss is best reproduced with the thermal conductivity method.

2.3 Evaluation of ice-constraining methods

The time evolution of the annual Arctic sea-ice area in ALB, THCD, TARGET and CTRL are displayed in Fig. 3 (left). In the CTRL simulations, there is a weak drift with increasing Arctic sea-ice extension, but it remains small compared to internal variability. The annual sea-ice areas of ALB and THCD are declining gradually at a rate comparable to that of the TARGET simulation. The results are similar when focusing on summer or winter (Fig. S2). This contrasts with previous studies that found an abrupt sea-ice decline after sea-ice albedo modification, as in Blackport and Kushner (2016) or Liu and Fedorov (2019). In ALB and THCD, the decline is gradual because the perturbation is small. Indeed, reducing the albedo with a stronger value (70%) simulates an abrupt decline, where the September sea-ice disappears within 5 years (Fig. S3).

Figure 3 (right) compares the seasonal cycles of the Arctic SIA for the different ensembles. The values for both ALB and THCD remain close to that of TARGET for all months. When investigating the differences with TARGET, only May and June in THCD are different from TARGET at the 90% confidence level. We also note that the sea-ice loss is slightly underestimated in February-March for ALB (and THCD), which is consistent with the smaller sensitivity of the JFM SIA illustrated in Fig. 2. The annual (September) sea-ice extent is 9.8 10^6 km^2 (5.4 10^6 km^2) in CTRL and 7.5 10^6 km^2 (2.5 10^6 km^2) in the two reduced-ice ensembles which correspond to a 23% (53%) reduction. Also, the sea-ice loss equal to 0.9 10^6 km^2 (~7 %) during December-January-February (DJF). Figure 4 compares the spatial patterns of the reduction of winter (DJF) and summer (JJA, from June to August) Arctic sea-ice concentration (SIC) in TARGET, ALB, and THCD. The spatial distributions of the sea-ice retreat are relatively similar, especially between ALB and THCD in winter (and spring; not shown): sea-ice melts mostly in the Barents, Labrador and Chukchi Seas. Compared to TARGET, more ice melts in the Barents Sea in ALB and THCD, and less in the Labrador Sea. In summer, the Arctic sea-ice melts almost everywhere with a minimum around the Queen Elizabeth Islands, with only subtle differences between the ensembles.

The similar seasonal sea-ice areas in the two reduced-ice ensembles hide larger differences in sea-ice

thickness (Fig. 5, left). While ALB weakly underestimates the ice thickness compared to TARGET, THCD has a significantly reduced seasonality. During winter and spring, THCD has thinner ice than ALB or TARGET, while in summer it has slightly more. ALB strongly melts the surface sea-ice in summer when the incoming shortwave surface radiation is largest, and THCD decreases the basal sea-ice growth in winter (as less ocean heat is transferred to sea-ice). In summer, changing thermal conductivity has limited consequences. Indeed, the heat flux in the sea-ice is small, as the sea-ice is isothermal. In both cases, the sea-ice reduction persists and reemerges in the next season, owing to coupled interactions among sea-ice thickness, sea-ice concentration and ocean temperature (Blanchard-Wrigglesworth et al., 2011a). For both ALB and THCD, the greatest thinning occurs where sea-ice is thickest (Central Arctic; not shown), following the growth-thickness feedback described in Bitz et al. (2004). In ALB and THCD, a thinner snow layer above ice is simulated throughout the year when compared to CTRL (Fig. 5, right). This is explained by a larger snow melting rate, as the snow-to-ice conversion is similar to CTRL (not shown). In ALB, the Arctic snow thickness resembles that of TARGET, except in spring when more incoming solar radiation rapidly melts the snow. THCD underestimates snow thickness throughout the year, possibly because, when the thermal conductivity is reduced, more heat is available to melt the snow.

To illustrate how the atmosphere/ocean exchanges are modified, Fig. 6 presents the total surface heat flux (short-wave, long-wave, sensible and latent fluxes; positive downward) over the Arctic. In the Central and Western Arctic, all three ensembles show anomalous downward heat flux into the ocean, but with different amplitudes: ALB overestimates while THCD underestimates the heat flux compared to TARGET (see also Fig. S4, top-left). This is mostly explained by the differences in surface albedo resulting in different short-wave absorption. Note that the surface albedo in THCD also decreases over sea-ice (much less than in ALB; not shown) due to the reduction of sea-ice and snow thicknesses. Most total surface heat flux differences between ALB and THCD are found off Queen Elisabeth Islands (Fig. 4, bottom). This coincides with the location of multiyear ice, where summer sea-ice albedo is important. As the sea-ice retreats in the Barents and Chukchi Seas, the winter oceanic heat loss strengthens near the sea-ice edges (Fig. 6, top), mostly due to sensible and

289 latent heat fluxes (not shown). Over the sea-ice edges, the ALB and THCD ensembles exhibit
290 similar heat flux changes as they have similar sea-ice losses.
291
292 The area-weighted surface heat flux without short-wave (i.e. turbulent and long-wave fluxes; Fig. 6,
293 bottom-left) and near-surface air temperature (Fig. 6, bottom-right), averaged north of 70°N display
294 negative (upward) anomalous heat flux and warmer temperatures for TARGET, ALB and THCD
295 throughout the year. The annual-mean warming is significantly more pronounced in ALB (1.63°C
296 north of 70°N) than in THCD (1.16°C north of 70°N; Fig S4, top-right). The radiative budget at the
297 top of the atmosphere (TOA) shows that the incoming shortwave radiation flux north of 70°N is
298 doubled in ALB when compared to THCD (not shown). Consistently, the net downwelling
299 shortwave radiative fluxes increase at the surface, so that the total downward heat flux in the
300 Canadian Archipelago in ALB is larger than in THCD (Fig. S4, top-left).
301 The Arctic warming is seasonally dependent. Even though the sea-ice cover shows its largest
302 reduction in summer, the warming over the polar cap in TARGET is maximum in autumn. This
303 lagged seasonal response, which is reproduced in ALB and THCD, is caused by the upward
304 turbulent fluxes over the newly opened water, as found previously (Serreze et al., 2007; Screen et
305 al., 2010; Deser et al. 2010b; Screen et al., 2013; Blackport and Kushner, 2016; Yoshimori et al.,
306 2018; England et al., 2018). In spring, ALB produces another warm peak, which is significantly
307 distinct from TARGET. April sea-ice concentration is very similar among ALB, THCD and
308 TARGET (not shown). The warming mainly occurs near Queen Elisabeth Islands where multiyear
309 sea-ice is located (not shown), which is likely related to the albedo reduction. The THCD ensemble
310 is colder in winter, as the reduced conductivity leads to a decreased heat conduction through the ice.
311 As a consequence, ALB is warmer than THCD, which lead to larger outgoing longwave radiation.

312 **3. Arctic and North Atlantic responses**

313 3.1. Winter atmospheric changes

314 Atmospheric changes occurring over the North Atlantic are shown for winter, one-to-three months

after the maximum heat flux anomalies. Figure 7 (top) displays the DJF sea level pressure (SLP) changes in ALB and THCD. In ALB, there are broad anticyclonic anomalies over Northern Siberia/Eastern Arctic and Greenland, and a low-pressure anomaly over the North Atlantic. This pattern projects on the negative phase of the NAO. We also see an anticyclonic anomaly in the Northern Pacific, near the west coast of North America, which is discussed in section 4. In THCD, a similar pattern is simulated, but with much weaker amplitude, so that the anomalies are not significant except off west America and above Greenland. As sea-ice loss produces enhanced warming in the lower troposphere (Deser et al., 2010b; Cattiaux and Cassou, 2013), we also show the geopotential height at 500 hPa (Z500; Fig. 7, bottom) to illustrate the mid-tropospheric changes. A broad anticyclonic anomaly appears over the North Pole, consistent with low-tropospheric warming in both ALB and THCD. The negative Z500 anomaly over the North Atlantic is only slightly significant in ALB, while the positive anomaly is significant off the northwestern coast of North America in ALB and THCD. An investigation of the difference between ALB and THC in winter further indicates a significant barotropic anticyclone in North Siberia (Fig. S4, bottom-middle), which is consistent with the anomalous downward heat flux in autumn in this region (Fig. S4, top-middle). A significant depression over Eurasia is also found (Fig. S4, bottom-middle). The negative NAO-like pattern is significantly stronger in ALB compared to THCD (Fig. S4, bottom-left) due to the stronger Arctic warming which enhances the pole-to-equator gradient temperature. At 50-hPa, in the lower stratosphere, ALB shows a weaker polar vortex than THCD (Fig. S4, bottom-right). Weak polar vortex anomalies classically propagate downward and are followed by negative Arctic Oscillation (AO) events in winter (Hartmann et al., 2000; Baldwin and Dunkerton, 1999; Baldwin et al. 2003; Kidston et al., 2015). Therefore, it is likely that the stratospheric changes also contribute to the stronger negative NAO-like anomalies in ALB when compared to THCD. Nevertheless, such influence on the NAO may be larger in early spring, as found by Sun et al., (2015).

Figure 8 displays the DJF zonal-mean temperature and winds over the North Atlantic sector (80°W-

20°E). A clear temperature increase in lower to mid-troposphere is simulated above the Arctic (60°N-90°N) as heat is released from the ocean. ALB undergoes a higher and larger Arctic warming, reaching about 400-hPa compared to 600-hPa for THCD. Significant warming in the troposphere is also seen between 20°N-40°N up to 200-hPa in both simulations. Weak warming is found in the free tropical troposphere, resembling what would produce a mini-global warming. The lower stratosphere north of 60°N is only modified in THCD, with a significant cooling. Consistent with the weaker meridional temperature gradient, the zonal wind weakens north of 55°N from the surface up to 100-hPa. The North Atlantic subtropical jet core is amplified around 40°N, 200-hPa. However, the winds are weaker in the equatorward flank of the jet (30°N to 0°N). For both ensembles, westerlies at 850-hPa are shifted south in the North Atlantic sector, as the meridional temperature gradient weakens north of 50°N. The global zonal-mean (not only Atlantic) winds also show an amplified subtropical jet, but with a small northward shift (not shown). In section 4, we see that this difference is consistent with the anomalies simulated over the Pacific Ocean.

3.2 Oceanic response

In the ocean, changes induced by melting sea-ice are less seasonal and therefore depicted here as annual-mean changes. Figure 9 presents the ocean temperature changes averaged over the upper 300 m. The Arctic warms near the summer sea-ice edges, as new open waters have a smaller surface albedo and allow more incoming solar radiation. A small cooling is simulated in the Barents and Greenland Seas, where the winter oceanic cooling of the ocean is amplified as sea-ice retreats (Fig. 4, top), which is detailed below.

Figure 10 displays oceanic properties for ALB only, as THCD results are similar, albeit with smaller magnitude (Fig. S5). In the Central Arctic, salinity decreases (Fig. 10, left) and the Beaufort gyre intensifies (Fig. 10, middle). The cause of these two related features might be the decreased freshwater export toward the North Atlantic, especially through ice transport at Fram Strait, as shown by Zhang et al. (2016). On the contrary, a positive salt anomaly is seen around the Eastern Arctic (Barents, Kara, Laptev, East Siberian, Chukchi Seas), possibly caused by a larger inflow of

North Atlantic water into the Arctic. In the Barents Sea, the 0-300 m temperature decreases slightly, (Fig. 9), but the top 100 m warms. As the salinity increases (Fig 10, left), the overall density stratification is reduced, which can lead to increased mixing and a release of the Arctic subsurface heat, consistently with the cooling of the 0-300m layer. These changes are due mostly to anomalous horizontal advection rather than to surface fluxes (not shown). The barotropic stream function also shows a negative anomaly north of the Barents Sea (Fig. 10, middle), consistent with a northward extension of the Norwegian current bringing more salt up to the north of Barents Sea. All these changes are consistent with the so-called “Atlantification” found in observations (Årthun et al., 2012; Polyakov et al., 2017; Lind et al. 2018). It suggests that such a process is linked to the Arctic sea-ice loss.

In Central North Atlantic, a cold and fresh anomaly is simulated along the North Atlantic current (around 45°N) while warm and salty anomalies are found in the subpolar gyre (see Figs. 9 and 10). These changes are consistent with the southward shift of the surface westerlies found previously. This shift of the westerlies can impact the ocean through the changes of the wind speed and its impacts on turbulent heat fluxes (Deser et al., 2010a; Suo et al. 2017) and by forcing an “inter-gyre gyre” (Marshall et al., 2001) through a shift of the wind stress curl and Ekman pumping (Fig. 10, middle). Indeed, we found that an anomalous gyre is found between Newfoundland and the British Isles (Fig. 10, center), which cools and decreases the salinity in the southern subpolar gyre by anomalous advection.

For both reduced sea-ice ensembles, the seawater density is slightly reduced over the 0-300 m layer in the north branch of the subpolar gyre. However, while the surface reduction is due to warming, deeper density changes are due to a fresh anomaly found in the Greenland Sea, downstream of the outflow of Arctic water from Fram Strait. The mixed layer depth is shallower in the Greenland Sea and South of Iceland, at the location of the main deep water formation site in this model (see section 2.1.2). This is consistent with a weakening of the AMOC (see Fig. 11 and S6) that is maximum near 55°N. The AMOC at 55°N, computed by the maximum Atlantic meridional stream function

between 500m and 2500 m, indeed exhibits a steady slowdown with a mean weakening of about 0.8 Sv in ALB.

4. Global-scale response

The sea surface temperature (SST) anomalies induced by sea-ice loss in ALB (Fig. 12, left) indicate significant warming both in the South Tropical Atlantic (0°S-20°S) and in the subtropical North Atlantic (20°N-40°N). The SST changes in the subtropical southeast Pacific are similar but more significant than those in Wang et al. (2018) who analyzed the impact of Arctic sea-ice loss in the first decades using the ghost forcing method. The Atlantic pattern is consistent with a decrease of the AMOC (Figs. 11 and S6), which brings less heat from the Southern Hemisphere to the North Atlantic (Latif et al., 2006; Mignot et al., 2007; Keenlyside et al., 2008; Kageyama et al., 2009). Besides, the decrease of low-cloud cover in the Southern Atlantic amplifies the warming (not shown). The North Pacific presents broad warming extending to the western American coasts, with a maximum north of the Kuroshio Extension. In the South Pacific, the SST pattern resembles the South Pacific Meridional mode (Zhang et al., 2014), with cooling from 10 to 30°S in the Central-East Pacific and warming from 20°S to 40°S in the Central-West Pacific. A cooling band is also simulated at 60°S. The THCD ensemble (Fig. 12, right) shows similar SST anomalies, except for a warming in the Gulf of Mexico and South Atlantic between 40°S and 50°S.

In ALB and THCD, the Z500 changes (Figs. 13 and S7, top-left) indicate a weakening of the Aleutian Low, anticyclonic anomalies centred over the South Pacific and a larger Amundsen Low. To illustrate the changes in the large-scale tropical atmospheric circulation, the 200-hPa velocity potential was calculated (Figs. 13 and S7, top-right). This shows the regions of large-scale ascents for negative velocity potential and descents for positive values, smoothing the smaller scales apparent in the vertical velocity. In CTRL, ascents are simulated over the Maritime continent and the Indo-Pacific warm pool (Figs. 13 and S7, top-right, contours) and descents occur from Eastern

Pacific to Africa. With reduced sea-ice extent, the Walker cell is shifted westward with more ascent from the Indian Ocean to the Gulf of Guinea and more descent in the Central and Eastern Pacific Ocean. Even though there is no significant SST cooling in the equatorial Pacific, ALB shows a small equatorial east Pacific cooling with an enhanced zonal SST gradient across the equatorial Pacific. The associated atmospheric circulation anomalies, therefore, resemble those usually associated with La Niña (e.g. Sterl et al. 2007) or the cold Interdecadal Pacific Oscillation phase (Henley et al., 2015; Gastineau et al., 2019).

Previous work argued that, as Arctic sea-ice melts, the TOA incoming shortwave radiation into the Arctic increases and the inter-hemispheric northward energy transport should decrease when the climate is at equilibrium. This leads to an anomalous Hadley cell with northward cross-equatorial surface winds (Kang et al. 2008; Cvijanivic and Chang, 2013; Yoshimori et al., 2018; Wang et al. 2018), shifting the ITCZ northward. However, we found in ALB and THCD that the atmospheric meridional energy transport increases in both simulations from 40°S to 65°N (not shown), while south of 65°N the oceanic meridional energy transport decreases, as the AMOC decreases (Figs. 11 and S6). This leads to southward cross-equatorial surface winds in the equatorial Atlantic. A southward shift of the ITCZ is simulated in the Atlantic Ocean, as well as in the south Pacific convergence zone. Nevertheless, we also found intensified South Pacific trades winds (Figs. 13 and S7, bottom-left) and anomalous northward cross-equatorial winds are simulated in the Central and Eastern Pacific, as found by Wang et al. (2018) in the first decades of their simulations. This results in Hadley circulation changes that are small and insignificant (Fig. S8). We conclude that the atmospheric northward energy transport changes are complex, as the ocean is not in equilibrium.

We also note an increase of precipitation in Brazil and Northeast Australia and drier conditions in much of North America in boreal winter. The precipitation changes are consistent with the cross-equatorial wind changes and the Walker circulation anomalies, with a significant southward (northward) ITCZ shift in the Atlantic (Pacific) Ocean (Figs. 13 and S7, bottom-right). Besides, the SST in the Pacific tends to project on the negative phase of the IPO, even though not significant, is

also consistent with the increase of rain in Brazil (Villamayor et al., 2018). The decrease of precipitation over California is also seen by Cvijanovic et al. (2017) and explained by large-scale atmospheric reorganization due to Arctic sea-ice loss. Lastly, the annual precipitation response also shows a southward shift of the South Pacific Convergence Zone.

5. Conclusion and Discussion

We investigate the influence of Arctic sea-ice loss on both local and global climate using the IPSL-CM5A2 model. We focus on the fast transient responses, occurring within 20 years following 10 years of adjustment. We study a relatively moderate Arctic sea-ice loss, corresponding to a 20% (50%) annual (September) sea-ice extent reduction. Two different methods are implemented to melt the Arctic sea-ice from a control simulation (CTRL) to assess the robustness of the associated climate impacts: reducing the sea-ice and snow above it by altering their albedo (in ALB) or thermal conductivity (in THCD). We adjust their values in order to reproduce the targeted summer Arctic sea-ice area. The resulting sea-ice areas and sea-ice concentration patterns are largely similar in TARGET, ALB and THCD. However, an underestimation of the winter sea-ice loss is systematically produced when reducing the albedo, while thermal conductivity reduction is more able to reproduce the target sea-ice area in both winter and summer. Most previous studies also found that decreasing the albedo leads to overestimated winter sea-ice (Deser et al., 2015; Blackport and Kushner, 2016; Screen et al., 2018; Sun et al., 2020). The fact that the ensemble ALB only simulates a small underestimation of sea-ice loss in winter is consistent with the effect of internal variability.

The physical mechanisms reducing the ice are different in the two methods. While albedo modifies the incoming solar radiation, thermal conductivity modulates the transfer of heat from the ocean to the atmosphere, controlling the winter sea-ice growth. This induces significant local differences even if the mean Arctic sea-ice areas are similar. For the reduced albedo simulations, there is a

stronger and less confined Arctic warming, especially in spring (as in Blackport and Kushner, 2016), when sea-ice cover is large. The thermal conductivity method simulates a thinner sea-ice and snow in winter/spring due to reduced air-sea fluxes.

The climate responses are mostly similar with the two methods. However, the magnitude of the anomalies is larger in the Northern Hemisphere with the albedo ensemble (ALB). Nonetheless, the Tropical and Southern Hemisphere SST and SLP responses in South Atlantic and South Pacific are of similar magnitude or larger in THCD. The origin of these small differences between the two methods remains to be understood using larger ensembles to increase to signal to noise ratio.

The Arctic sea-ice loss creates a positive sea level pressure anomaly over Northern Siberia and a negative anomaly in the Central Atlantic in winter, resembling a negative NAO-like pattern. In winter, the North Atlantic lower-tropospheric jet (the eddy-driven jet) is shifted southward which is consistent with the reduced low-tropospheric temperature gradient and the simulated negative NAO-like pattern (Screen et al., 2018). The subtropical jet in the North Atlantic is also shifted southward. However, the global mean zonal-wind shows a small northward shift, due to a strong Pacific contribution. At 40°N, the zonal mean changes are dominated by the weakening of the Aleutian Low in the Pacific. Even though the warming mostly occurs near the surface, the SLP and Z500 over the Arctic have a barotropic structure, suggesting strong eddy-mean flow interactions, as found in Deser et al. (2016) and Wang et al. (2018).

In the past few decades, the Arctic Ocean freshwater content has increased, which has been explained by the accumulation of freshwater from sea-ice melt and river runoff. Zhang et al. (2016) linked this accumulation to less sea-ice export as the Beaufort gyre has intensified. This is consistent with our study as the Beaufort gyre intensifies, while its salinity decreases. In the observations, the reason for the spin-up of the gyre has been linked to an anomalous anticyclone over the Beaufort gyre (Giles et al., 2012). In our study, such anomalous anticyclone is absent (not shown), therefore further investigation would be needed to quantify the mechanisms for the

Beaufort gyre intensification. In addition, the salinity increases in the Barents Sea due to stronger North Atlantic inflow. This is consistent with the so-called Atlantification that is usually invoked to explain sea-ice variability (Årthun et al., 2012; Polyakov et al. 2017; Barton et al., 2018; Lind et al. 2018). Our results suggest that Atlantification could be amplified by Arctic sea-ice loss within two or three decades. The freshwater and heat exchanges between the Arctic and North Atlantic are modified. The subtropical gyre shifts south and an intergyre gyre develops due to wind changes (Marshall et al., 2001). The AMOC decreases, which is associated with a shallower mixed layer at the main convection site. According to previous studies, Arctic sea-ice loss might play a dominant role in AMOC weakening. For instance, Sévellec et al. (2017) suggested that 75% of the observed AMOC decline is driven by Arctic sea-ice changes and Sun et al. (2018) found that about 50% of AMOC decline produced at the end of the 21st century in a scenario simulation is due to Arctic sea-ice loss. However, the relative importance of surface heat and freshwater flux in weakening the AMOC in future climate is still an open question. There is a cold and fresh anomaly in the mid-latitude around 45°N, which resembles the projected warming minimum (or warming hole) in the subpolar North Atlantic (Collins et al., 2013) and has been linked to AMOC decrease (Drijfhout et al, 2012; Sévellec et al., 2017; Suo et al., 2017; Sun et al. 2018). However, as ALB and THCD show different magnitude of ocean surface cooling (respectively 0.3 °C and 0.08°C) with the same intensity of weakening of the AMOC, we suggest that most of the changes are associated with the southward shift of the westerlies. Lastly, the Atlantic is warmer at 0°S-25°S, which is consistent with the AMOC weakening (Mignot et al., 2007).

Even if the equatorial Indo-Pacific shows no significant change associated with sea-ice loss, warming is simulated in the South subtropical Pacific around 30°S, encircled by cooling around 20°S and 60°S. The pattern resembles the South Pacific meridional mode (Zhang et. al., 2014). It also broadly resembles a cold IPO (Henley et al., 2015; Gastineau et al., 2019) but with no significant anomalies in the equatorial band. The cooling around 20°S and South Atlantic warming is associated with a westward shift of the Walker cells, with more ascent over the Atlantic and more

descent over the Pacific. This suggests that the fast decadal response to sea-ice loss is dominated by the sea-ice-driven AMOC changes in the Atlantic, which are then driving the Pacific changes through atmospheric bridges, although the causality was not fully determined. It would be consistent with previous works where that Atlantic warming leads to a cold IPO phase through modification of the Walker cells (Li et al. 2016; Ruprich-Robert et al. 2017; Martin-Rey et al., 2018). However, such mechanism found here might be model-dependent. For instance, Wang et al. (2018) found a large influence of the North subtropical ocean, while in our case the South Atlantic is key.

Previous studies found that sea-ice loss is typically associated with a “mini-global warming” at equilibrium, after several decades of oceanic circulation adjustment. However, in this paper, the transient changes after a 10-yr adjustment to sea-ice loss show contrasting results, with a North Pacific warming and a Southeast Pacific cooling, somewhat resembling those found in the transient studies of Cvijanovic et al. (2017) and Wang et al. (2018). The reason for the different response in the Pacific is an open question. The ocean dynamics could be an important aspect. Wang et al. (2018) find indeed as smaller warming in a climate model fully coupled than coupled with an ocean mixed layer, especially in Northern Hemisphere. Furthermore, the oceanic initial state was not varied in our simulations, although it could affect the transient response (Sévellec and Federov, 2017; Germe et al., 2018). Lastly, as suggested by Monerie et al. (2018) and Smith et al. (2017), the response to Arctic sea-ice loss could also depend on the mean state. As different components (ice, AMOC, global temperature) have different adjustment scales, the global response could change over time. We argue that the fast response to the sea-ice loss of the coming decades could be quite different from the equilibrium response to sea-ice loss (Liu and Federov, 2019). This could be clarified by coordinated sensitivity experiments with different climate models.

Acknowledgements

This research was supported by the Blue-Action project (European Union's Horizon 2020 research and innovation programme, grant number: 727852). This work was granted access to the HPC resources of TGCC under the allocation A5-0107403 and A3-0107403 made by GENCI. We thank the three anonymous reviewers for their useful comments and suggestions.

References

Årthun, M., Eldevik, T., Smedsrud, L. H., Skagseth, Ø., & Ingvaldsen, R. B. (2012). Quantifying the influence of Atlantic heat on Barents sea-ice variability and retreat. *Journal of Climate*, *25*(13), 4736-4743.

Aumont, O., & Bopp, L. (2006). Globalizing results from ocean in situ iron fertilization studies. *Global Biogeochemical Cycles*, 20(2).

Baldwin, M. P., & Dunkerton, T. J. (1999). Propagation of the Arctic Oscillation from the stratosphere to the troposphere. *Journal of Geophysical Research*: Atmospheres, 104(D24), 30937-30946.

Baldwin, M. P., Stephenson, D. B., Thompson, D. W., Dunkerton, T. J., Charlton, A. J., & O'Neill, A. (2003). Stratospheric memory and skill of extended-range weather forecasts. Science, 301(5633), 636-640.

Barton, B. I., Lenn, Y. D., & Lique, C. (2018). Observed Atlantification of the Barents Sea causes the Polar Front to limit the expansion of winter sea-ice. *Journal of Physical Oceanography*, *48*(8), 1849-1866.

Bitz, C. M., & Roe, G. H. (2004). A mechanism for the high rate of sea ice thinning in the Arctic Ocean. *Journal of Climate*, *17*(18), 3623-3632.

Blackport, R., & Kushner, P. J. (2016). The transient and equilibrium climate response to rapid summertime sea-ice loss in CCSM4. *Journal of Climate*, *29*(2), 401-417.

581 Blackport, R., & Kushner, P. J. (2017). Isolating the atmospheric circulation response to Arctic sea-
582 ice loss in the coupled climate system. *Journal of Climate*, *30*(6), 2163-2185.
583 Blackport, R., & Screen, J. A. (2019). Influence of Arctic sea ice loss in autumn compared to that in
584 winter on the atmospheric circulation. *Geophysical Research Letters*, *46*(4), 2213-2221.
585 Blanchard-Wrigglesworth, E., Armour, K. C., Bitz, C. M., & DeWeaver, E. (2011a). Persistence and
586 inherent predictability of Arctic sea-ice in a GCM ensemble and observations. *Journal of Climate*,
587 *24*(1), 231-250.
588 Cassano, E. N., Cassano, J. J., Higgins, M. E., & Serreze, M. C. (2014). Atmospheric impacts of an
589 Arctic sea ice minimum as seen in the Community Atmosphere Model. *International Journal of*
590 *Climatology*, *34*(3), 766-779.
591 Cattiaux, J., & Cassou, C. (2013). Opposite CMIP3/CMIP5 trends in the wintertime Northern
592 Annular Mode explained by combined local sea ice and remote tropical influences. *Geophysical*
593 *research letters*, *40*(14), 3682-3687.
594 Cavalieri, D. J., C. L. Parkinson, P. Gloersen, and H. J. Zwally. 1996, updated yearly. *Sea Ice*
595 *Concentrations from Nimbus-7 SMMR and DMSP SSM/I-SSMIS Passive Microwave Data, Version*
596 *1*. [Indicate subset used]. Boulder, Colorado USA. NASA National Snow and Ice Data Center
597 Distributed Active Archive Center. doi: https://doi.org/10.5067/8GQ8LZQVL0VL.
598 Cohen, J., Screen, J. A., Furtado, J. C., Barlow, M., Whittleston, D., Coumou, D., ... & Jones, J.
599 (2014). Recent Arctic amplification and extreme mid-latitude weather. *Nature geoscience*, *7*(9), 627
600 Collins, M., Knutti, R., Arblaster, J., Dufresne, J. L., Fichefet, T., Friedlingstein, P., ... & Shongwe,
601 M. (2013). Long-term climate change: projections, commitments and irreversibility. In *Climate*
602 *Change 2013-The Physical Science Basis: Contribution of Working Group I to the Fifth Assessment*
603 *Report of the Intergovernmental Panel on Climate Change* (pp. 1029-1136). Cambridge University
604 Press.
605 Cunningham, S. A., Kanzow, T., Rayner, D., Baringer, M. O., Johns, W. E., Marotzke, J., ... &
606 Meinen, C. S. (2007). Temporal variability of the Atlantic meridional overturning circulation at 26.5
607 N. *science*, *317*(5840), 935-938.

Cvijanovic, I., & Chiang, J. C. (2013). Global energy budget changes to high latitude North Atlantic cooling and the tropical ITCZ response. *Climate dynamics*, *40*(5-6), 1435-1452.

Cvijanovic, I., Caldeira, K., & MacMartin, D. G. (2015). Impacts of ocean albedo alteration on Arctic sea-ice restoration and Northern Hemisphere climate. *Environmental Research Letters*, *10*(4), 044020

Cvijanovic, I., Santer, B. D., Bonfils, C., Lucas, D. D., Chiang, J. C., & Zimmerman, S. (2017). Future loss of Arctic sea-ice cover could drive a substantial decrease in California's rainfall. *Nature communications*, *8*(1), 1-10.

Deser, C., Alexander, M. A., Xie, S. P., & Phillips, A. S. (2010a). Sea surface temperature variability: Patterns and mechanisms. *Annual review of marine science*, *2*, 115-143.

Deser, C., Tomas, R., Alexander, M., & Lawrence, D. (2010b). The seasonal atmospheric response to projected Arctic sea-ice loss in the late twenty-first century. *Journal of Climate*, *23*(2), 333-351

Deser, C., Tomas, R. A., & Sun, L. (2015). The role of ocean–atmosphere coupling in the zonal-mean atmospheric response to Arctic sea-ice loss. *Journal of Climate*, *28*(6), 2168-2186.

Deser, C., Sun, L., Tomas, R. A., & Screen, J. (2016). Does ocean coupling matter for the northern extratropical response to projected Arctic sea-ice loss?. *Geophysical Research Letters*, *43*(5), 2149-2157.

Drijfhout, S., Van Oldenborgh, G. J., & Cimatoribus, A. (2012). Is a decline of AMOC causing the warming hole above the North Atlantic in observed and modeled warming patterns?. *Journal of Climate*, *25*(24), 8373-8379.

Dufresne, J. L., Foujols, M. A., Denvil, S., Caubel, A., Marti, O., Aumont, O., ... & Bony, S. (2013). Climate change projections using the IPSL-CM5 Earth System Model: from CMIP3 to CMIP5. *Climate Dynamics*, *40*(9-10), 2123-2165.

England, M., Polvani, L., & Sun, L. (2018). Contrasting the Antarctic and Arctic atmospheric responses to projected sea ice loss in the late twenty-first century. *Journal of Climate*, *31*(16), 6353-6370.

England, M., L. Polvani, L. Sun and C. Deser, 2020: Tropical climate responses to projected Arctic and Antarctic sea ice loss. Nat. Geosci., accepted, doi: 10.1038/s41561-020-0546-9.

Fichefet, T., & Maqueda, M. M. (1997). Sensitivity of a global sea-ice model to the treatment of ice thermodynamics and dynamics. *Journal of Geophysical Research: Oceans*, *102*(C6), 12609-12646.

Fichefet, T., & Maqueda, M. M. (1999). Modelling the influence of snow accumulation and snow-ice formation on the seasonal cycle of the Antarctic sea-ice cover. *Climate Dynamics*, *15*(4), 251-268.

García-Serrano, J., Frankignoul, C., Gastineau, G., & de La Càmara, A. (2015). On the predictability of the winter Euro-Atlantic climate: lagged influence of autumn Arctic sea-ice. *Journal of Climate*, *28*(13), 5195-5216.

Gastineau, G., Friedman, A. R., Khodri, M., & Vialard, J. (2019). Global ocean heat content redistribution during the 1998–2012 Interdecadal Pacific Oscillation negative phase. Climate dynamics, 53(1-2), 1187-1208.

Germe, A., Sévellec, F., Mignot, J., Fedorov, A., Nguyen, S., & Swingedouw, D. (2018). The impacts of oceanic deep temperature perturbations in the North Atlantic on decadal climate variability and predictability. *Climate Dynamics*, *51*(5-6), 2341-2357.

Giles, K. A., Laxon, S. W., Ridout, A. L., Wingham, D. J., & Bacon, S. (2012). Western Arctic Ocean freshwater storage increased by wind-driven spin-up of the Beaufort Gyre. *Nature Geoscience*, *5*(3), 194-197.

Hartmann, D. L., Wallace, J. M., Limpasuvan, V., Thompson, D. W., & Holton, J. R. (2000). Can ozone depletion and global warming interact to produce rapid climate change?. *Proceedings of the National Academy of Sciences*, *97*(4), 1412-1417.

Henley, B. J., Gergis, J., Karoly, D. J., Power, S., Kennedy, J., & Folland, C. K. (2015). A tripole index for the interdecadal Pacific oscillation. Climate Dynamics, 45(11-12), 3077-3090.

Hourdin, F., Foujols, M. A., Codron, F., Guemas, V., Dufresne, J. L., Bony, S., ... & Braconnot, P. (2012). Climate and sensitivity of the IPSL-CM5A coupled model: impact of the LMDZ atmospheric grid configuration. *Clim. Dynam., online first: doi*, *10*.

Kageyama, M., Merkel, U., Otto-Bliesner, B., Prange, M., Abe-Ouchi, A., Lohmann, G., ... & Zhang, X. (2013). Climatic impacts of fresh water hosing under Last Glacial Maximum conditions: a multi-model study. *Climate of the Past*, *9*(2), 935-953.

Kang, S. M., Held, I. M., Frierson, D. M., & Zhao, M. (2008). The response of the ITCZ to extratropical thermal forcing: Idealized slab-ocean experiments with a GCM. *Journal of Climate*, *21*(14), 3521-3532.

Keenlyside, N. S., Latif, M., Jungclaus, J., Kornblueh, L., & Roeckner, E. (2008). Advancing decadal-scale climate prediction in the North Atlantic sector. *Nature*, *453*(7191), 84.

Kidston, J., Scaife, A. A., Hardiman, S. C., Mitchell, D. M., Butchart, N., Baldwin, M. P., & Gray, L. J. (2015). Stratospheric influence on tropospheric jet streams, storm tracks and surface weather. *Nature Geoscience*, *8*(6), 433.

King, M. P., Hell, M., & Keenlyside, N. (2016). Investigation of the atmospheric mechanisms related to the autumn sea-ice and winter circulation link in the Northern Hemisphere. *Climate dynamics*, *46*(3-4), 1185-1195.

Kirchmeier-Young, M. C., Zwiers, F. W., & Gillett, N. P. (2017). Attribution of extreme events in Arctic sea ice extent. *Journal of Climate*, 30(2), 553-571.

Krinner, G., Viovy, N., de Noblet-Ducoudré, N., Ogée, J., Polcher, J., Friedlingstein, P., ... & Prentice, I. C. (2005). A dynamic global vegetation model for studies of the coupled atmosphere-biosphere system. *Global Biogeochemical Cycles*, *19*(1).

Latif, M., Böning, C., Willebrand, J., Biastoch, A., Dengg, J., Keenlyside, N., ... & Madec, G. (2006). Is the thermohaline circulation changing?. *Journal of Climate*, *19*(18), 4631-4637.

Li, X., Xie, S. P., Gille, S. T., & Yoo, C. (2016). Atlantic-induced pan-tropical climate change over the past three decades. *Nature Climate Change*, *6*(3), 275-279.

Lind, S., Ingvaldsen, R. B., & Furevik, T. (2018). Arctic warming hotspot in the northern Barents Sea linked to declining sea-ice import. *Nature climate change*, *8*(7), 634-639.

Liu, W., & Fedorov, A. V. (2019). Global impacts of Arctic sea-ice loss mediated by the Atlantic meridional overturning circulation. *Geophysical Research Letters*, *46*(2), 944-952.

Madec, G. (2008). the Nemo team (2008) NEMO ocean engine. *Note du Pôle de modélisation. Institut Pierre-Simon Laplace (IPSL), France*. [Available online at http://www.nemo-ocean.eu/content/download/5302/31828/file/NEMO_book.pdf.]

Magnusdottir, G., Deser, C., & Saravanan, R. (2004). The effects of North Atlantic SST and sea-ice anomalies on the winter circulation in CCM3. Part I: Main features and storm track characteristics of the response. *Journal of Climate*, *17*(5), 857-876.

Marshall, J., Johnson, H., & Goodman, J. (2001). A study of the interaction of the North Atlantic Oscillation with ocean circulation. *Journal of Climate*, *14*(7), 1399-1421.

Martín-Rey, M., Polo, I., Rodríguez-Fonseca, B., Losada, T., & Lazar, A. (2018). Is there evidence of changes in tropical Atlantic variability modes under AMO phases in the observational record?. *Journal of Climate*, 31(2), 515-536.

Maslowski, W., Clement Kinney, J., Higgins, M., & Roberts, A. (2012). The future of Arctic sea-ice. *Annual Review of Earth and Planetary Sciences*, *40*, 625-654.

Masson-Delmotte, V., Zhai, P., Pörtner, H. O., Roberts, D., Skea, J., Shukla, P. R., ... & Connors, S. (2018). Global warming of 1.5 C. *An IPCC Special Report on the impacts of global warming of 1.5°C above pre-industrial levels and related global greenhouse gas emission pathways, in the context of strengthening the global response to the threat of climate change, sustainable development, and efforts to eradicate poverty*

McCusker, K. E., Kushner, P. J., Fyfe, J. C., Sigmond, M., Kharin, V. V., & Bitz, C. M. (2017). Remarkable separability of circulation response to Arctic sea-ice loss and greenhouse gas forcing. *Geophysical Research Letters*, *44*(15), 7955-7964.

Mignot, J., Ganopolski, A., & Levermann, A. (2007). Atlantic subsurface temperatures: Response to a shutdown of the overturning circulation and consequences for its recovery. *Journal of Climate*, *20*(19), 4884-4898.

Monerie, P. A., Oudar, T., & Sanchez-Gomez, E. (2019). Respective impacts of Arctic sea-ice decline and increasing greenhouse gases concentration on Sahel precipitation. *Climate dynamics*, *52*(9-10), 5947-5964.

715 Oudar, T., Sanchez-Gomez, E., Chauvin, F., Cattiaux, J., Terray, L., & Cassou, C. (2017).
716 Respective roles of direct GHG radiative forcing and induced Arctic sea-ice loss on the Northern
717 Hemisphere atmospheric circulation. *Climate dynamics*, *49*(11-12), 3693-3713.
718 Overland, J. E., & Wang, M. (2013). When will the summer Arctic be nearly sea ice free?.
719 *Geophysical Research Letters*, *40*(10), 2097-2101.
720 Peings, Y., & Magnusdottir, G. (2014). Response of the wintertime Northern Hemisphere
721 atmospheric circulation to current and projected Arctic sea-ice decline: A numerical study with
722 CAM5. *Journal of Climate*, *27*(1), 244-264.
723 Polyakov, I. V., Pnyushkov, A. V., Alkire, M. B., Ashik, I. M., Baumann, T. M., Carmack, E. C., ...
724 & Krishfield, R. (2017). Greater role for Atlantic inflows on sea-ice loss in the Eurasian Basin of
725 the Arctic Ocean. *Science*, *356*(6335), 285-291.
726 Pörtner, H. O., Roberts, D., Masson-Delmotte, V., Zhai, P., Tignor, M., Poloczanska, E., ... &
727 Petzold, J. (2019). IPCC Special Report on the Ocean and Cryosphere in a Changing Climate.
728 *IPCC Intergovernmental Panel on Climate Change: Geneva, Switzerland*.
729 Ruprich-Robert, Y., Msadek, R., Castruccio, F., Yeager, S., Delworth, T., & Danabasoglu, G. (2017).
730 Assessing the climate impacts of the observed Atlantic multidecadal variability using the GFDL
731 CM2. 1 and NCAR CESM1 global coupled models. *Journal of Climate*, *30*(8), 2785-2810.
732 Schweiger, A., R. Lindsay, J. Zhang, M. Steele, H. Stern, Uncertainty in modeled arctic sea ice
733 volume, J. Geophys. Res., doi:10.1029/2011JC007084, 2011
734 Screen, J. A., & Simmonds, I. (2010). Increasing fall-winter energy loss from the Arctic Ocean and
735 its role in Arctic temperature amplification. *Geophysical Research Letters*, *37*(16).
736 Screen, J. A., Simmonds, I., Deser, C., & Tomas, R. (2013). The atmospheric response to three
737 decades of observed Arctic sea ice loss. *Journal of Climate*, *26*(4), 1230-1248.
738 Screen, J. A., Deser, C., Simmonds, I., & Tomas, R. (2014). Atmospheric impacts of Arctic sea-ice
739 loss, 1979–2009: Separating forced change from atmospheric internal variability. *Climate dynamics*,
740 *43*(1-2), 333-344.
741 Screen, J. A., Deser, C., Smith, D. M., Zhang, X., Blackport, R., Kushner, P. J., ... & Sun, L. (2018).

742 Consistency and discrepancy in the atmospheric response to Arctic sea-ice loss across climate
743 models. *Nature Geoscience*, *11*(3), 155.
744 Sepulchre, P., Caubel, A., Ladant, J.-B., Bopp, L., Boucher, O., Braconnot, P., Brockmann, P.,
745 Cozic, A., Donnadieu, Y., Estella-Perez, V., Ethé, C., Fluteau, F., Foujols, M.-A., Gastineau, G.,
746 Ghattas, J., Hauglustaine, D., Hourdin, F., Kageyama, M., Khodri, M., Marti, O., Meurdesoif, Y.,
747 Mignot, J., Sarr, A.-C.,
748 Seierstad, I. A., & Bader, J. (2009). Impact of a projected future Arctic sea ice reduction on
749 extratropical storminess and the NAO. *Climate dynamics*, *33*(7-8), 937.
750 Serreze, M. C., Holland, M. M., & Stroeve, J. (2007). Perspectives on the Arctic's shrinking sea-ice
751 cover. *Science*, *315*(5818), 1533-1536.
752 Sévellec, F., Fedorov, A. V., & Liu, W. (2017). Arctic sea-ice decline weakens the Atlantic
753 meridional overturning circulation. *Nature Climate Change*, *7*(8), 604.
754 Singarayer, J. S., Bamber, J. L., & Valdes, P. J. (2006). Twenty-first-century climate impacts from a
755 declining Arctic sea-ice cover. *Journal of Climate*, *19*(7), 1109-1125.
756 Simon, A., Frankignoul, C., Gastineau, G., & Kwon, Y. O. (2020). An Observational Estimate of the
757 Direct Response of the Cold-Season Atmospheric Circulation to the Arctic Sea Ice Loss.
758 *Journal of Climate*, *33*(9), 3863-3882.
759 SIMIP Community (2020). Arctic sea ice in CMIP6. Geophysical Research Letters, 47,
760 e2019GL086749. https://doi.org/10.1029/2019GL086749
761 Smith, D. M., Dunstone, N. J., Scaife, A. A., Fiedler, E. K., Copsey, D., & Hardiman, S. C. (2017).
762 Atmospheric response to Arctic and Antarctic sea-ice: The importance of ocean–atmosphere
763 coupling and the background state. *Journal of Climate*, *30*(12), 4547-4565.
764 Sterl, A., van Oldenborgh, G. J., Hazeleger, W., & Burgers, G. (2007). On the robustness of ENSO
765 teleconnections. *Climate Dynamics*, *29*(5), 469-485.
766 Stocker, T. F., Qin, D., Plattner, G. K., Tignor, M., Allen, S. K., Boschung, J., ... & Midgley, P. M.
767 (2013). Climate change 2013: The physical science basis. *Contribution of working group I to the*
768 *fifth assessment report of the intergovernmental panel on climate change*, *1535*.

Strey, S. T., Chapman, W. L., & Walsh, J. E. (2010). The 2007 sea-ice minimum: Impacts on the Northern Hemisphere atmosphere in late autumn and early winter. *Journal of Geophysical Research: Atmospheres*, *115*(D23).

Stroeve, J. C., Kattsov, V., Barrett, A., Serreze, M., Pavlova, T., Holland, M., & Meier, W. N. (2012). Trends in Arctic sea ice extent from CMIP5, CMIP3 and observations. *Geophysical Research Letters*, 39(16).

Suo, L., Gao, Y., Guo, D., & Bethke, I. (2017). Sea-ice free Arctic contributes to the projected warming minimum in the North Atlantic. *Environmental Research Letters*, *12*(7), 074004.

Sun, L., C. Deser and R. A. Tomas, 2015: Mechanisms of stratospheric and tropospheric circulation response to projected Arctic sea ice loss. J. Climate, *28, 7824-7845, doi: 10.1175/JCLI-D-15-0169.1*.

Sun, L., Alexander, M., & Deser, C. (2018). Evolution of the global coupled climate response to Arctic sea ice loss during 1990–2090 and its contribution to climate change. *Journal of Climate*, *31*(19), 7823-7843

Sun, L., Deser, C., Tomas, R. A., & Alexander, M. (2020). Global coupled climate response to polar sea-ice loss: Evaluating the effectiveness of different ice-constraining approaches. *Geophysical Research Letters*, 47, e2019GL085788. https://doi.org/10.1029/2019GL085788

Tomas, R. A., Deser, C., & Sun, L. (2016). The role of ocean heat transport in the global climate response to projected Arctic sea ice loss. *Journal of Climate*, 29(19), 6841-6859.

Villamayor, J., Ambrizzi, T., & Mohino, E. (2018). Influence of decadal sea surface temperature variability on northern Brazil rainfall in CMIP5 simulations. *Climate dynamics*, *51*(1-2), 563-579.

Wang, K., Deser, C., Sun, L., & Tomas, R. A. (2018). Fast response of the tropics to an abrupt loss of Arctic sea ice via ocean dynamics. *Geophysical Research Letters*, *45*(9), 4264-4272.

Wassmann, P., Kosobokova, K. N., Slagstad, D., Drinkwater, K. F., Hopcroft, R. R., Moore, S. E., ... & Berge, J. (2015). The contiguous domains of Arctic Ocean advection: trails of life and death. *Progress in Oceanography*, *139*, 42-65.

Yoshimori, M., Abe-Ouchi, A., Tatebe, H., Nozawa, T., & Oka, A. (2018). The Importance of Ocean

Dynamical Feedback for Understanding the Impact of Mid–High-Latitude Warming on Tropical Precipitation Change. *Journal of Climate*, *31*(6), 2417-2434.

Zhang, H., Clement, A., & Di Nezio, P. (2014). The South Pacific meridional mode: A mechanism for ENSO-like variability. *Journal of Climate*, *27*(2), 769-783.

Zhang, J., Steele, M., Runciman, K., Dewey, S., Morison, J., Lee, C., ... & Toole, J. (2016). The Beaufort Gyre intensification and stabilization: A model-observation synthesis. *Journal of Geophysical Research: Oceans*, *121*(11), 7933-7952.

Figures

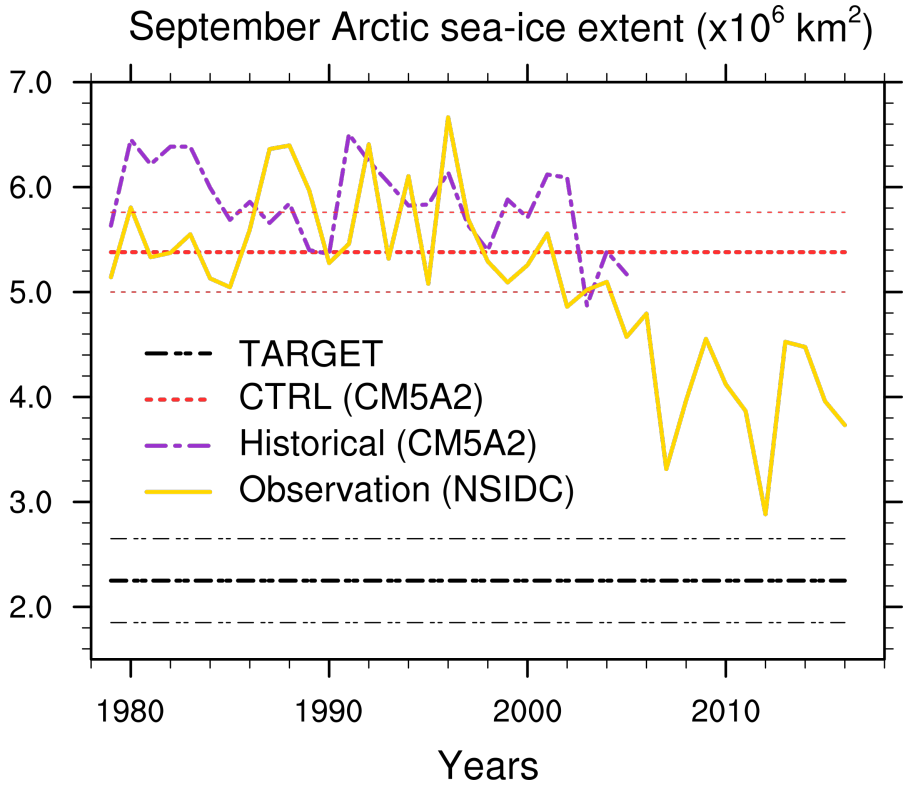

Figure 1: Time evolution of the September Arctic sea-ice extent in observation (calculated from NSIDC data; Cavalieri et al., 1996; yellow curve), and a historical run with IPSL-CM5A2 (purple line). The red (black) thick line shows the mean of the present-day CTRL ensemble (TARGET) and the red (black) thin lines display the two standard deviation error bar.

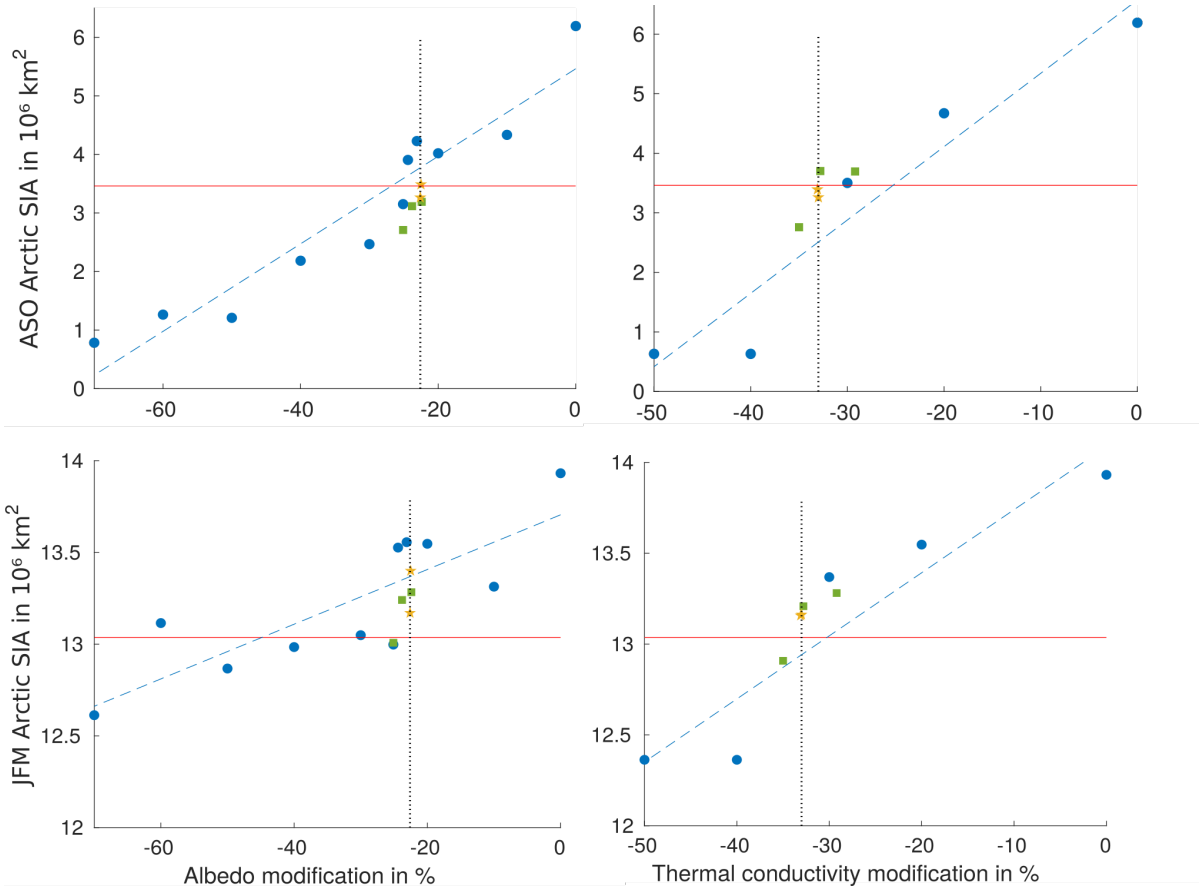

Figure 2: Mean Arctic sea-ice area (SIA) averaged over the months August-September-October (ASO; top) and over the months January-February-March (JFM; bottom), in 10^6 km^2, against the change in albedo (left) and thermal conductivity (right), in %. Results from single members are shown by blue dots together with its linear regression (dashed blue line). Results from 5-members ensembles and 10-members ensembles are shown by green squares and yellow stars respectively. The target (Arctic sea-ice area for the period 2035-2055 with CM5A) is indicated by the red line, and the reduction of albedo (22.6%) and thermal conductivity (33%) for the two experiments ALB and THCD respectively are indicated by dotted black lines.

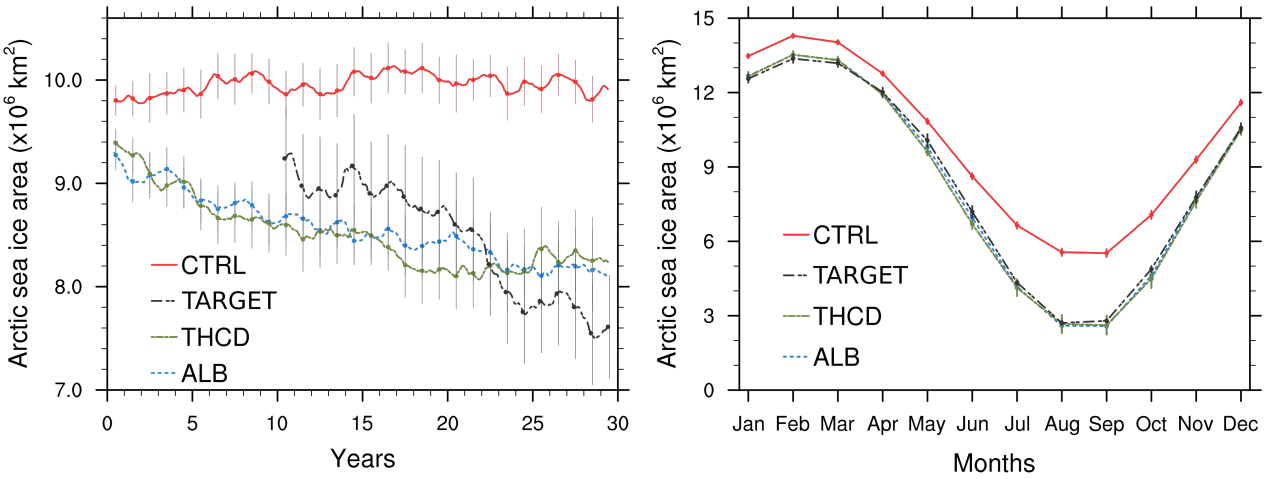

867 Figure 3: Time-series of the annual-mean Arctic sea-ice area, in 10^6 km^2 (left), and seasonal cycle averaged
868 over the years 10-30 (right), for TARGET (black line), CTRL (red line), ALB (blue line) and THCD (green
869 line) ensembles. Vertical bars indicate the 90% confidence intervals for the ensemble-means.

870

871

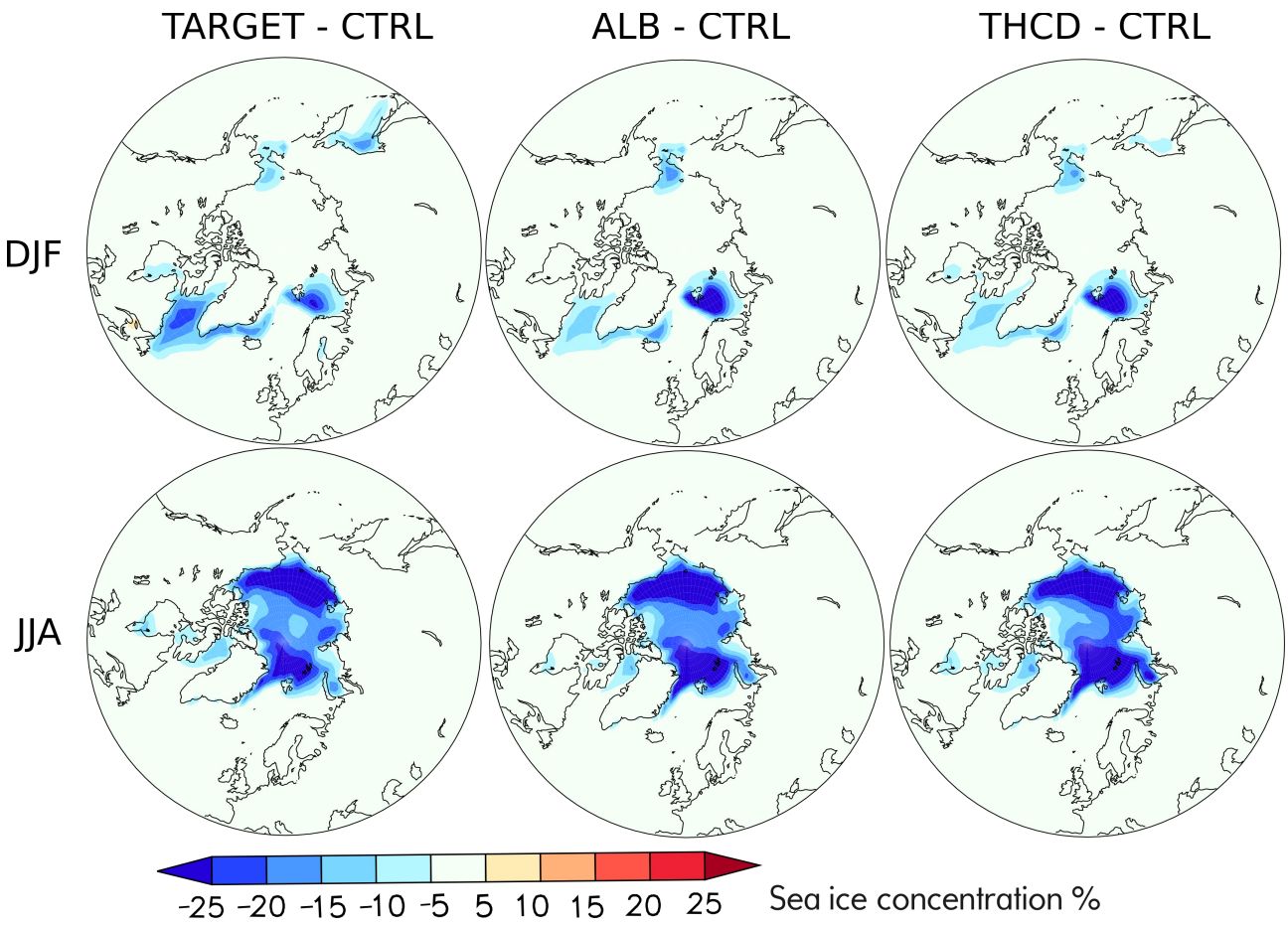

Figure 4: Difference in sea-ice concentration compared to the CTRL simulation, for TARGET (left), ALB (middle) and THCD (right), in %, averaged over December-January-February (DJF; top) and June-July-August (JJA; bottom).

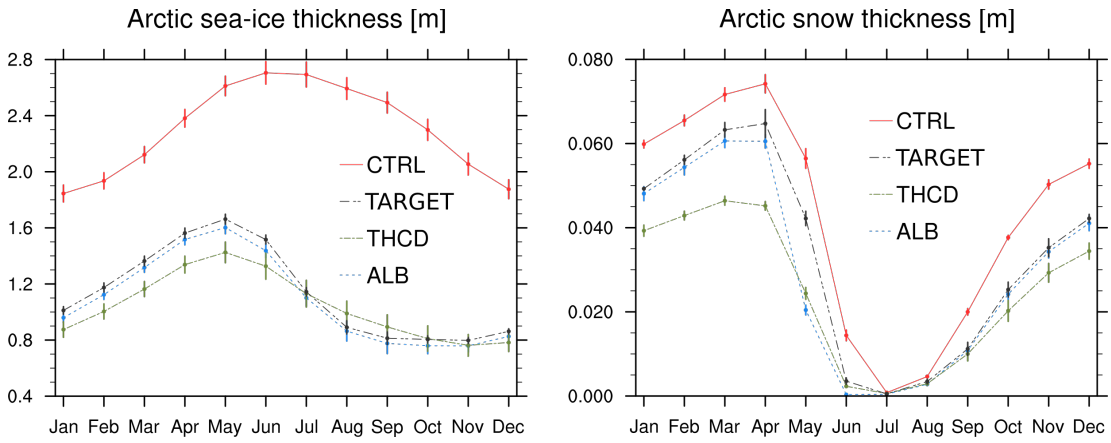

Figure 5: Seasonal cycle of Arctic sea-ice (left) and snow on sea-ice (right) thickness, in m, for CTRL (red), TARGET (black), ALB (blue) and THCD (green). Vertical bars indicate the 90% confidence interval for the ensemble-means.

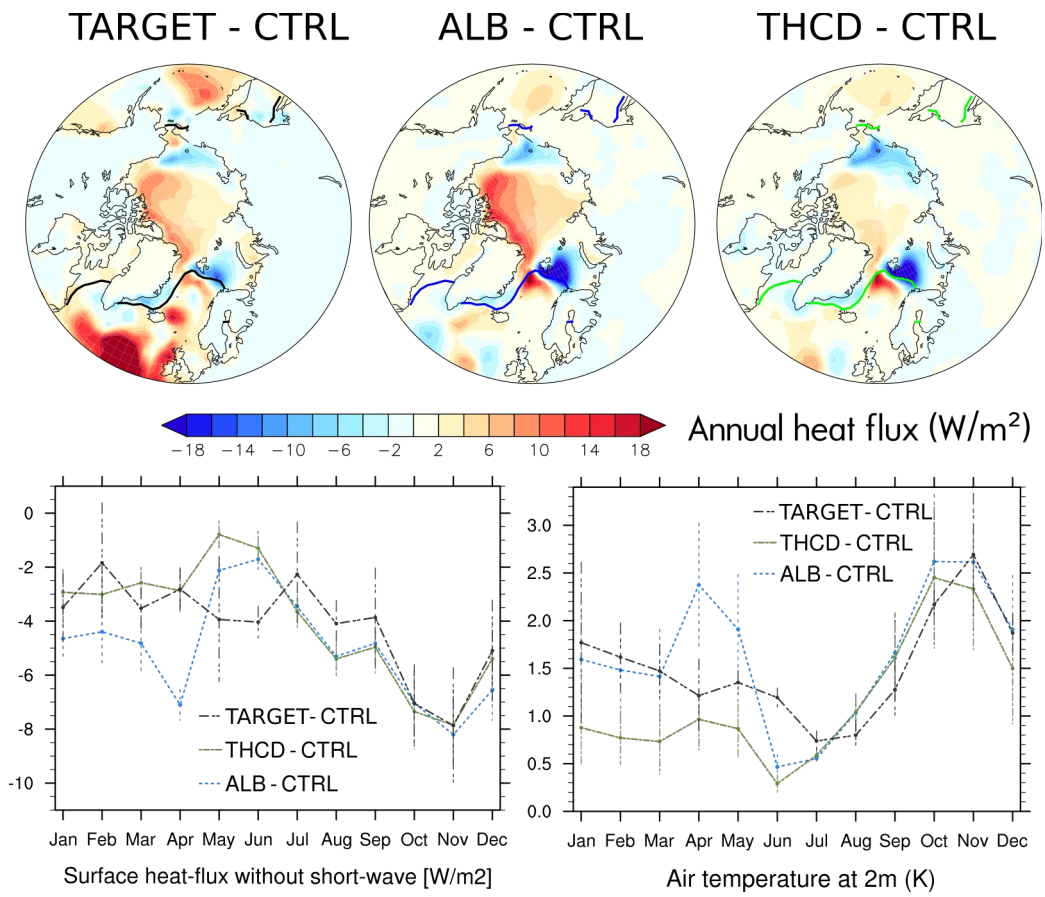

Figure 6: Anomalies of the annual-mean total heat flux with respect to CTRL (positive downward), in W/m^2 for TARGET (top-left), ALB (top-middle) and THCD (top-right). The lines indicate the sea-ice edge (i.e. 15 % in concentration threshold) for the corresponding ensemble (black for TARGET, blue for ALB and green for THCD). The signal north of this line is significant at the 90% confidence level. Mean seasonal cycle of the anomalies with respect to CTRL, averaged north of 70°N for the surface heat flux without short-wave (i.e, sensible, latent and long-wave heat fluxes; positive downward; bottom-left), in W/m² and air temperature at 2 m (bottom-right), in K. Bars illustrate the 90% confidence interval for the ensemble-mean.

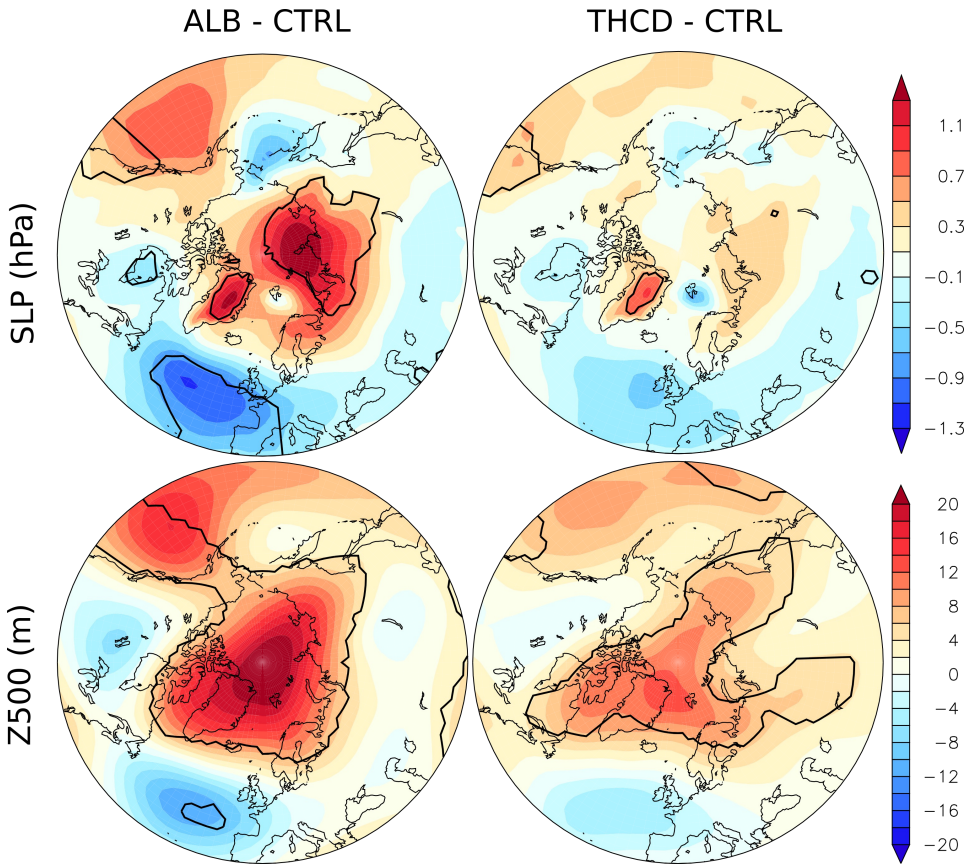

Figure 7: Anomalies of sea-level pressure (SLP; top), in hPa and geopotential height at 500 hPa (Z500; bottom), in m, averaged over December-January-February with respect to CTRL for ALB (left) and THCD (right). Black lines indicate the 90 % confidence level.

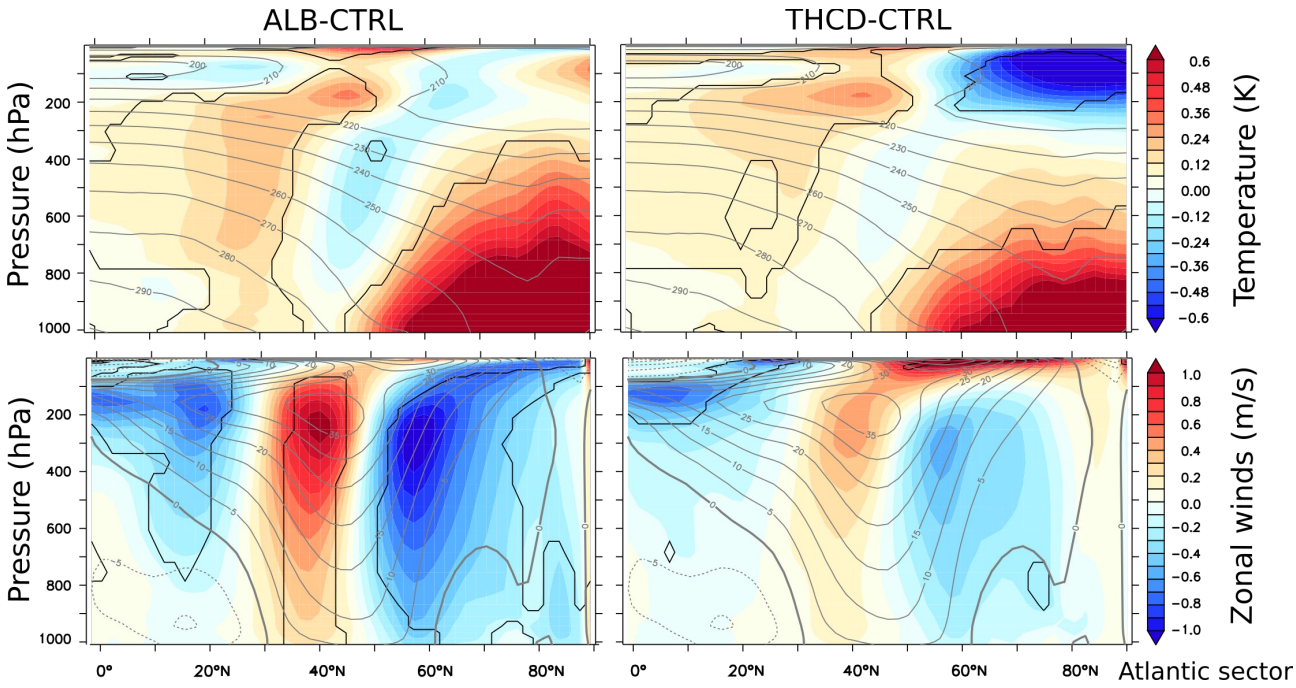

946 Figure 8: Anomalies of zonal-mean air temperature (top), in K, and zonal-mean zonal wind (bottom), in m/s,
947 averaged over December-January-February (DJF) and over the North Atlantic sector (80°W-20°E) with
948 respect to CTRL for ALB (left) and THCD (right). Grey contours indicate the climatology and black
949 contours show the 90 % confidence level.

950

951

952

953

954

955

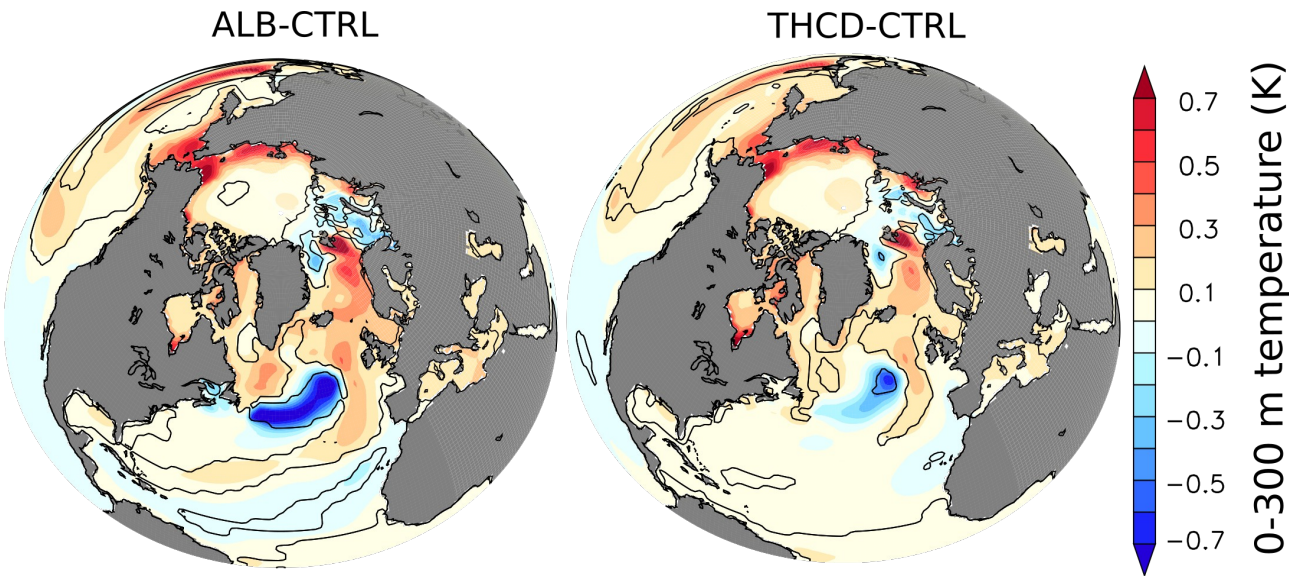

Figure 9: Anomalies of the annual-mean ocean temperature averaged over the upper 300 m, in K, with respect to CTRL for ALB (left) and THCD (right). The 90% confidence level is depicted by the black contours.

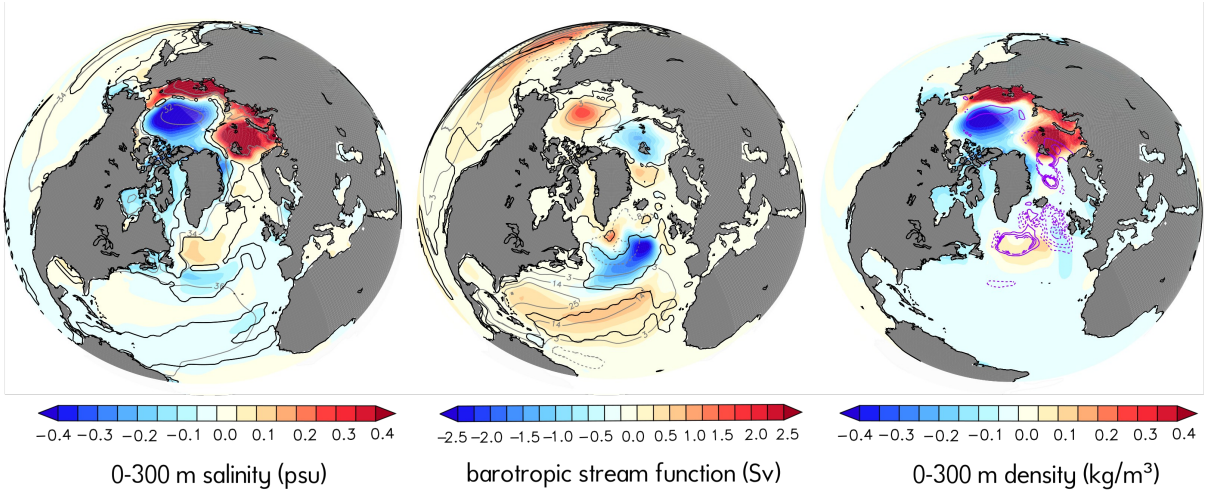

Figure 10: Anomalies of the annual-mean salinity averaged over the top 300 m of the ocean (left), in psu, of the barotropic stream function (middle; positive clockwise), in Sv, and of the density averaged over the top 300 m of the ocean (right) for ALB minus CTRL. Black contour defines the 90% confidence level, the mean CTRL value is in gray contour. In the right panel, the mixed layer depth difference for ALB minus CTRL is shown in purple line (dashed for negative) with the contour intervals as follow: (-140,-100,-60,-40,-20,20,60,100,140), in m.

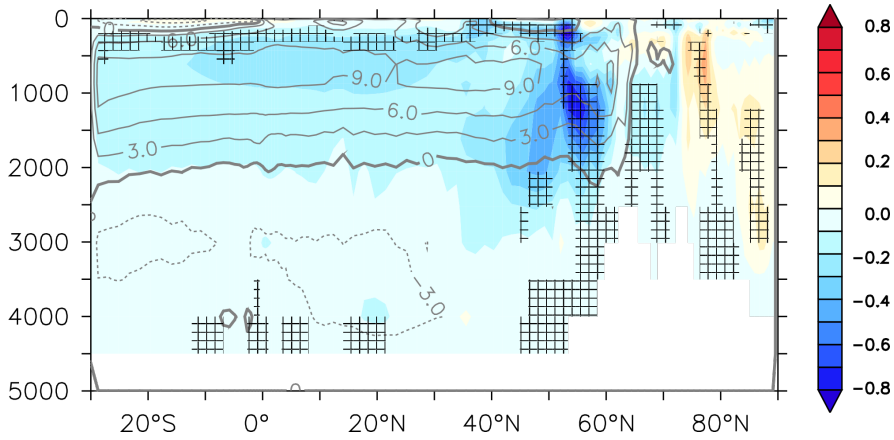

Figure 11: Anomalies of the Atlantic meridional stream function, for ALB minus CTRL, in Sv. The mean AMOC of the CTRL simulation is superimposed (grey contours; positive clockwise) and hashes illustrate the anomalies with a confidence level larger than 90%.

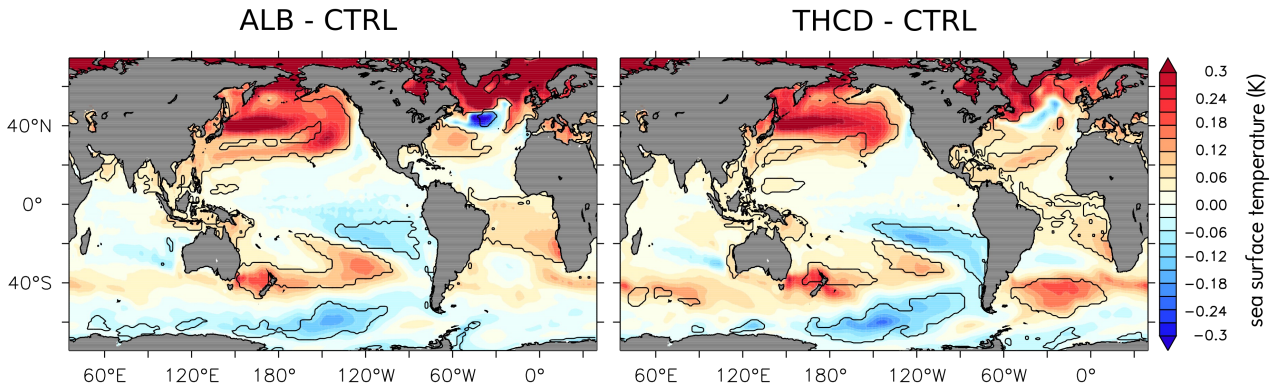

Figure 12: Anomalies of the annual-mean sea surface temperature, in K, with respect to CTRL for ALB (left) and THCD (right). Black contour shows the 90 % confidence level.

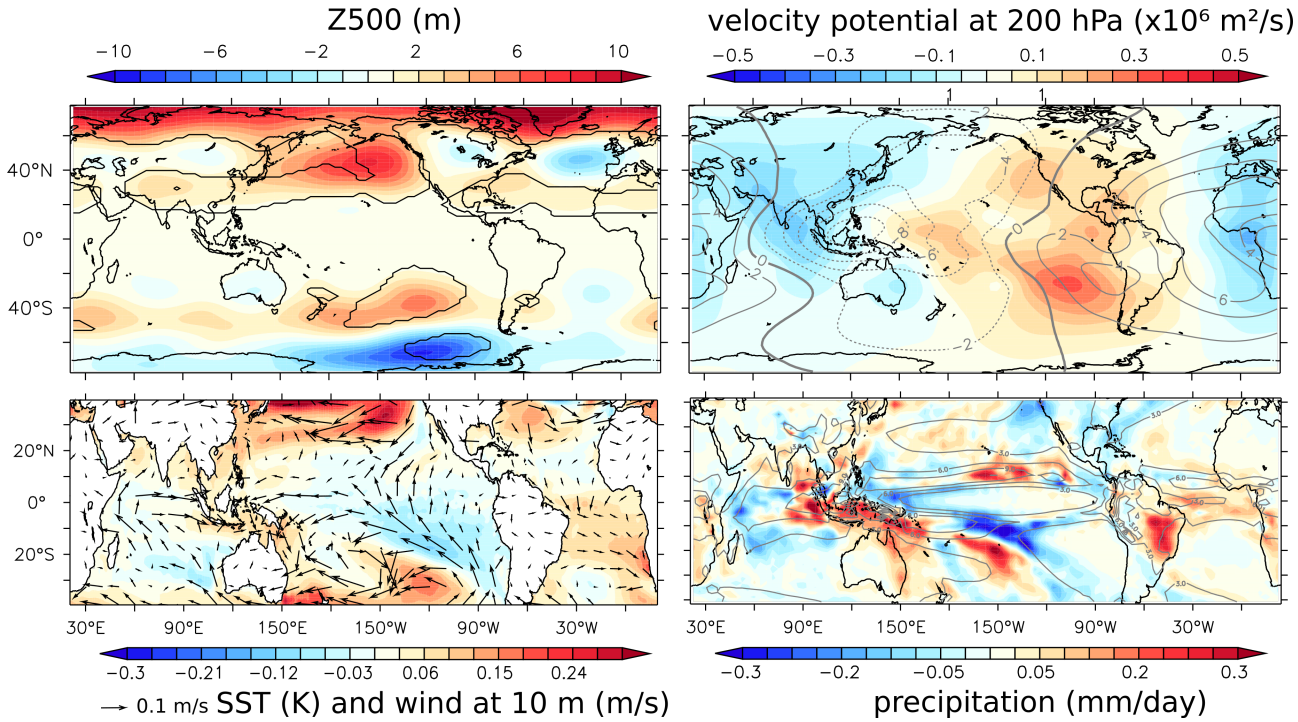

1024 Figure 13: Annual-mean anomalies of the geopotential height at 500 hPa (Z500; top-left), in m, velocity
1025 potential at 200 hPa (top-right), in 10^6 m^2/s, sea surface temperature, in K (shading) with the wind at 10 m
1026 (arrows; bottom-left), in m/s and precipitation (bottom-right), in mm/day, with respect to CTRL for ALB. In
1027 the upper left panel, the 90% confidence level is shown in black contour. The gray contour provides the
1028 corresponding value in CTRL in the right panels.

1029

1030

1031

1032

1033

1034

1035

1036

1037

1038

SUPPLEMENTARY FILES

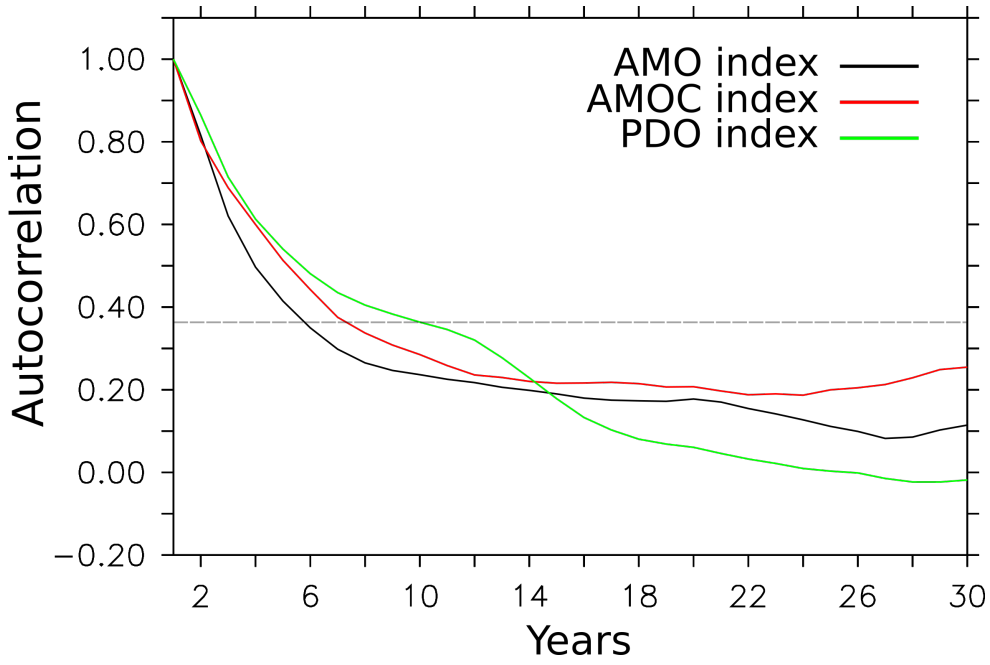

Figure S1: Autoregression of the AMO (Atlantic Multidecadal Oscillation) index (black), AMOC (Atlantic Meridional Overturning Circulation) index (red) and PDO (Pacific Decadal Oscillation) index (green) for a 2500 year pre-industrial control of the IPSLCM5A model (CMIP5). The AMO index is defined as monthly area-weighted SST* anomalies averaged over the North Atlantic (0:60°N, 80°W:0°E). The AMOC index is defined as the leading principal component (PC) of the annual averaged Atlantic meridional streamfunction (Sv) from 30°S to 90°N. The PDO index time-series is defined as the leading PC of monthly North Pacific (20:70°N, 110°E:100°W) area-weighted SST* anomalies. The SST* denotes that the global mean SST anomaly has been removed from the local SST anomalies at each time step. A 12-month running mean has been applied to the AMO and PDO times series. The grey dashed line indicates e^{-1} value to illustrate the e-folding time.

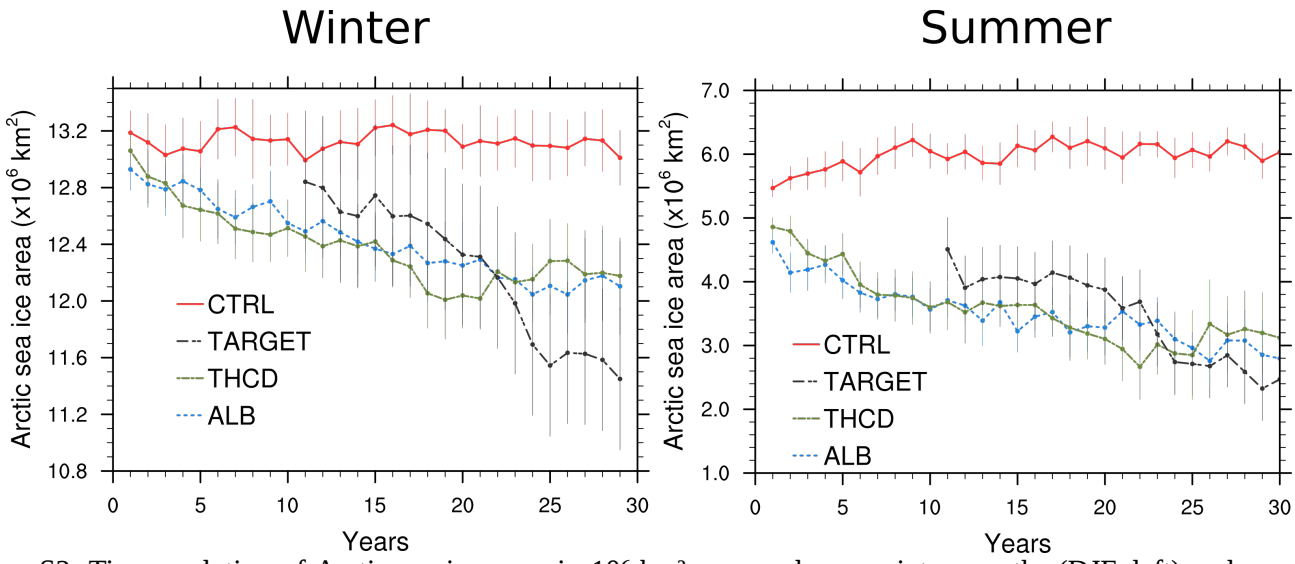

Figure S2: Time evolution of Arctic sea-ice area, in 10^6 km² averaged over winter months (DJF, left) and summer months (ASO; right), in TARGET (black line), CTRL (red line), ALB (blue line) and THCD (green line). Vertical bars indicate the 90% confidence intervals for the ensemble-means.

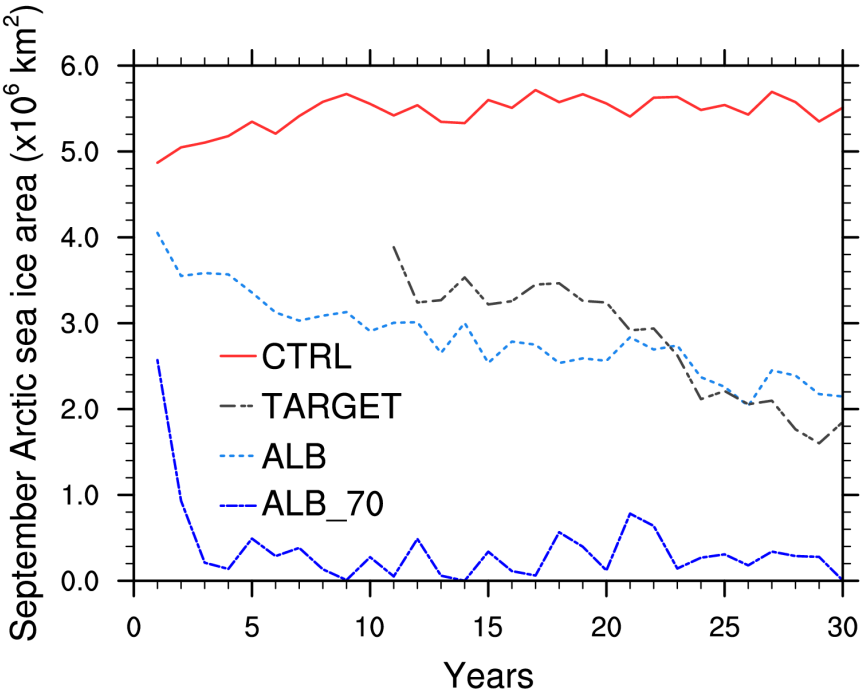

Figure S3: Time evolution of the September Arctic sea-ice area, in 10^6 km² for TARGET (black line), CTRL (red line), ALB (called here ALB_22.6, blue dotted line) ensembles and a single member similar to CTRL but with a reduction of the Northern Hemisphere sea-ice and snow albedo of 70%, called ALB_70 (blue line)

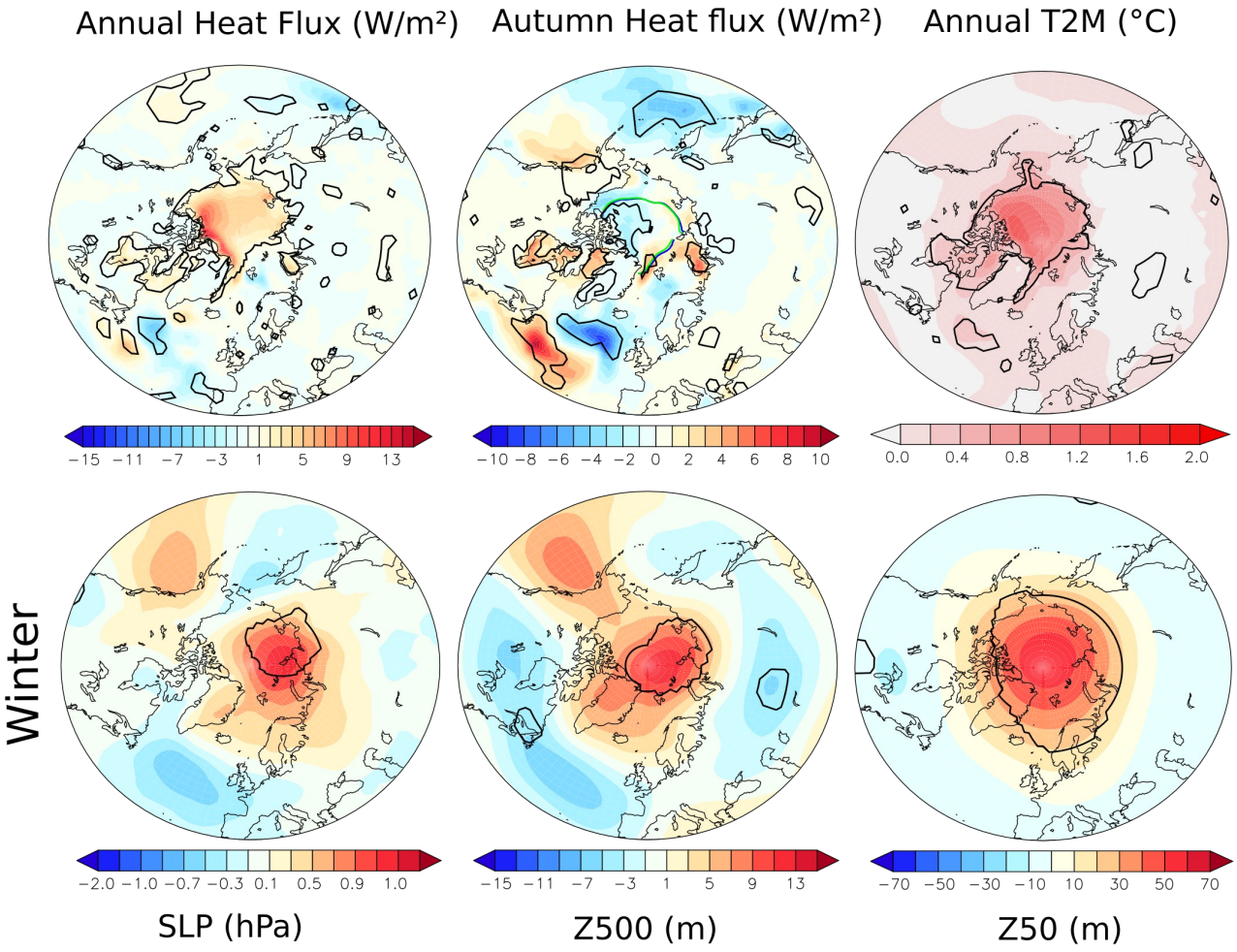

Figure S4: Difference between ALB and THCD for the annual heat flux (positive downward;top-left), the autumn heat flux (averaged over SON, September-October-November; top-middle), in W/m², the annual surface temperature (top-right), in °C, the winter (averaged over DJF, December-January-February) sea-level pressure (SLP) in hPa, geopotential height at 500 hPa, in m and the geopotential height at 50 hPa, in m. The 90% confidence level is shown in black contour.

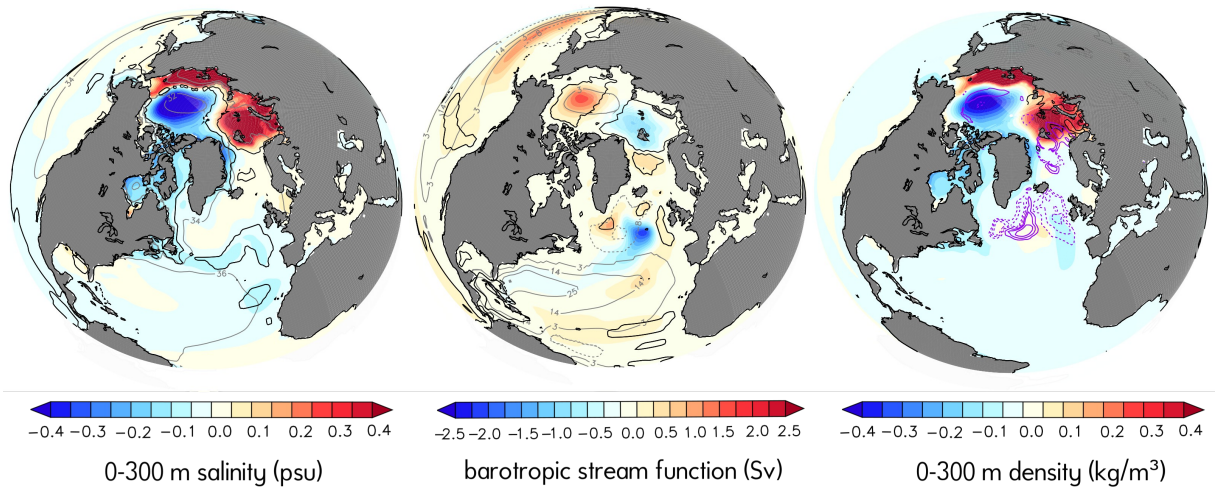

Figure S5: Same as Fig. 10, but for THCD.

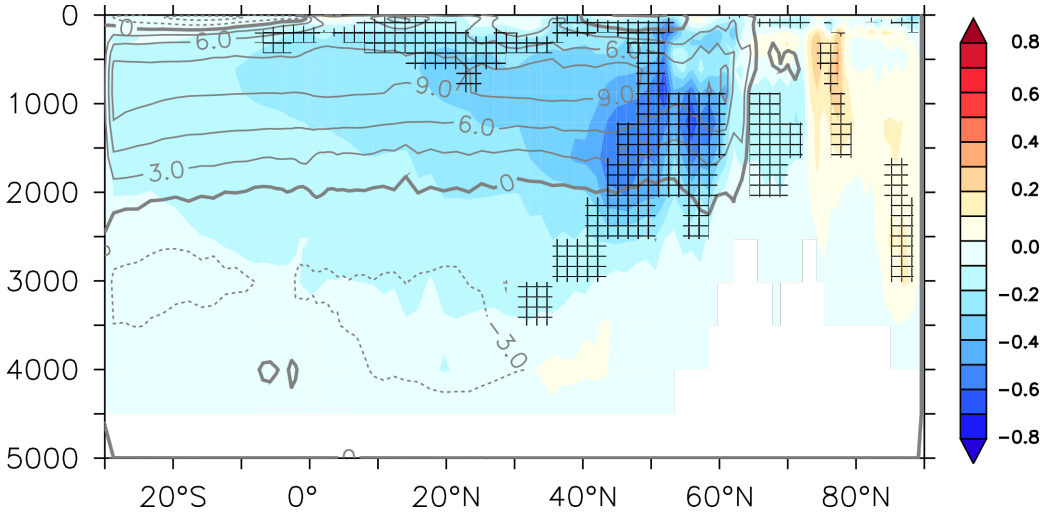

Figure S6: Same as Fig. 11, but for THCD

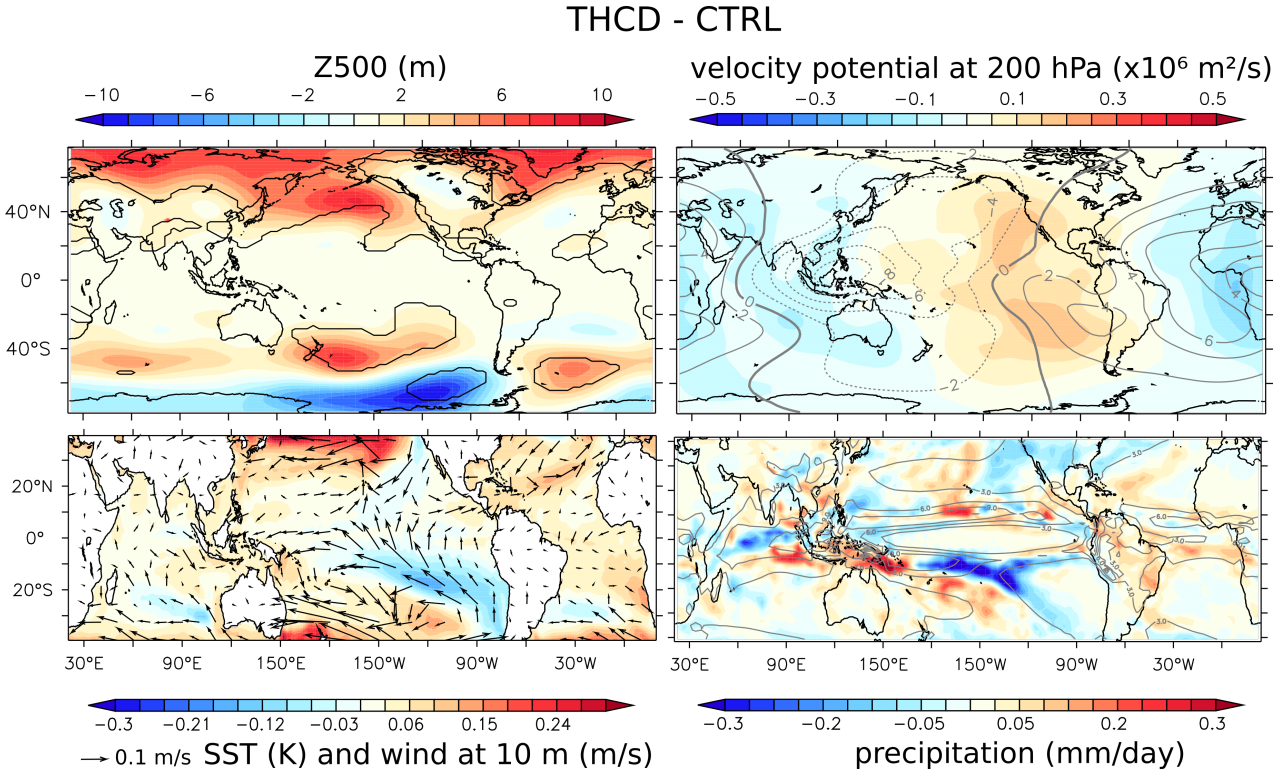

Figure S7: Same as Fig. 13, but for THCD.

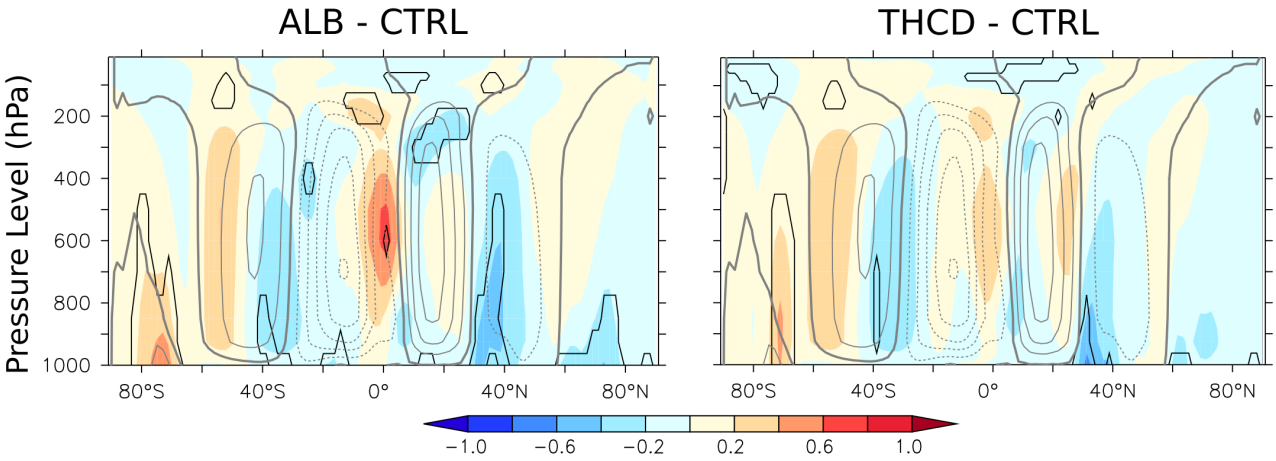

Figure S8: Annual-mean anomalies of meridional streamfunction (shading) in 10^{-9} kg/s with respect to CTRL for ALB (left) and THCD (right). The 90% confidence level is shown in grey contour and the mean CTRL value is in gray contour black contour (contour interval = 2 10^{9} kg/s)